Central Schemes for Nonconservative Hyperbolic Systems

M.J.Castro* Carlos Pares† Gabriella Puppo‡ Giovanni Russo§

May 18, 2012

Abstract

In this work we present a new approach to the construction of high order finite volume central schemes on staggered grids for general hyperbolic systems, including those not admitting a conservation form. The method is based on finite volume space discretization on staggered cells, central Runge-Kutta time discretization, and integration over a family of paths, associated to the system itself, for the generalization of the method to nonconservative systems. Applications to the one and the two layers shallow water models as prototypes of systems of balance laws and systems with source terms and nonconservative products respectively, will be illustrated.

1 Introduction

Shock capturing schemes for the numerical approximation of systems of conservation laws have been an active field of research for the last thirty years (see for example [25], [47], and [45]). Many papers have been also devoted to their extension to hyperbolic systems with source terms and/or nonconservative products putting special emphasis on the exact preservation of steady solutions (well-balanced property): see [3], [35] or [39].

In the particular case of systems of conservation laws, central schemes have the attractive feature of producing accurate results without requiring the solution of the Riemann problem. From the original second order scheme of Nessyahu and Tadmor [33], a considerable progress has been made, to produce general purpose, high order shock capturing schemes on staggered grids [40, 2] or [23] for the 2D case. See also [27]. Let us briefly recall the basis of these methods: we consider a system of conservation laws

$$u_t + f(u)_x = 0, \quad x \in \mathbb{R},\ t > 0. \tag{1.1}$$

where $u \in \mathbb{R}^m$, $f : \mathbb{R}^m \to \mathbb{R}^m$ is continuous and differentiable in $\mathbb{R}^m$. Let us consider computational cells $I_j = [x_{j-1/2}, x_{j+1/2}]$ with constant width Δx, and a constant time step Δt. Let us suppose that some approximations $\bar{u}_j^n$ of the cell averages of the sought weak solution are known at time $t^n = n\Delta t$. A high order reconstruction operator is then applied to these cell averages in order to obtain a piecewise smooth approximation of the solution at the time t^n:

$$u^n(x) = \sum_j R_j^n(x)\chi_{I_j}(x), \quad \forall x,$$

where χ_{I_j} is the characteristic function of the interval I_j. Thus the reconstruction is smooth in the interior of the cells, but it is in general discontinuous across cell interfaces. The reconstruction operator

*Universidad de Málaga, Málaga, Spain. castro@anamat.cie.uma.es

†Universidad de Malaga, Malaga, Spain. pares@anamat.cie.uma.es

‡Dipartimento di Matematica, Politecnico di Torino, Corso Duca degli Abruzzi 24, 10129 Torino, Italy. puppo@calvino.polito.it

§Dipartimento di Matematica ed Informatica, Università di Catania, Viale Andrea Doria 6, 95125 Catania, Italy. russo@dmi.unict.it

has to be essentially non-oscillatory: the reconstruction step should not introduce a significant increase of the total variation. Some examples of conservative, high order, essentially non-oscillatory reconstruction operators are MUSCL, ENO, WENO, PPM, or PHM (see [49], [20], [45], [46], [16], [28], [22]).

Next, as in Godunov-type methods, the initial value problem

$$\begin{cases} \tilde{u}_t + f(\tilde{u})_x = 0, \quad x \in \mathbb{R},\ t \in (t^n, t^{n+1}], \\ \\ \tilde{u}(x, t^n) = u^n(x), \quad x \in \mathbb{R}, \end{cases} \tag{1.2}$$

is considered. The difference with Godunov-type methods is that, instead of calculating or approximating the cell averages of the solution $\tilde{u}$ at cells I_j, the cell averages are updated on the staggered grid whose cells are given by $I_{j+1/2} = [x_j, x_{j+1}]$. The cell averages computed on the staggered grid

$$\bar{u}_{j+1/2}(t) = \frac{1}{\Delta x} \int_{I_{j+1/2}} \tilde{u}(x,t)\, dx$$

satisfy the equation:

$$\bar{u}'_{j+1/2} = -\frac{1}{\Delta x} \left[f(\tilde{u}(x_{j+1}, t)) - f(\tilde{u}(x_j, t)) \right]. \tag{1.3}$$

Notice that, if Δt is small enough, $\widetilde{u}$ is continuous at the center of the cells x_j and thus no exact or approximate Riemann solver is required to compute accurate numerical fluxes to approximate the right-hand side of (1.3). For the time integration, a Runge-Kutta method is applied to solve (1.3) with initial condition

$$\bar{u}_{j+1/2}(t^n) = \bar{u}^n_{j+1/2} = \frac{1}{\Delta x} \int_{x_j}^{x_{j+1}} u^n(x)\, dx = \frac{1}{\Delta x} \int_{x_j}^{x_{j+1/2}} R^n_j(x)\, dx + \frac{1}{\Delta x} \int_{x_{j+1/2}}^{x_{j+1}} R^n_{j+1}(x)\, dx.$$

The goal of this paper is to explore the possibility of extending this strategy to hyperbolic systems of balance laws

$$u_t + f(u)_x = S(u)\sigma_x, \tag{1.4}$$

or hyperbolic systems with source terms and nonconservative products

$$u_t + f(u)_x = B(u)u_x + S(u)\sigma_x, \tag{1.5}$$

where $u \in \mathbb{R}^m$, $f : \mathbb{R}^m \to \mathbb{R}^m$ is continuous and differentiable; $S : \mathbb{R}^m \to \mathbb{R}^m$ is continuous; B is a matrix-valued continuous function; and $\sigma : \mathbb{R} \to \mathbb{R}$ is a continuous and differentiable known function. Most PDE systems arising in fluid models have the form (1.4) or (1.5).

By adding the artificial equation

$$\sigma_t = 0,$$

(1.5) can be reformulated in the form

$$w_t + A(w)w_x = 0, \quad x \in \mathbb{R},\ t > 0, \tag{1.6}$$

with:

$$w = \begin{bmatrix} u \\ \sigma \end{bmatrix}, \quad A(w) = \begin{pmatrix} \nabla f(u) - B(u) & -S(u) \\ 0 & 0 \end{pmatrix}, \tag{1.7}$$

where $\nabla f(u)$ represents the Jacobian of the flux function. Therefore, we will consider the more general problem of extending the strategy of central schemes to hyperbolic systems of the form (1.6). The extended methods are expected to be well-balanced and to reduce to the conservative case whenever the source terms and the nonconservative products vanish. In particular, if some of the equations of the system are conservation laws (as it often happens), the method should be conservative for these equations. The advantages we expect from this approach consist in improved efficiency due to the minimal characteristic information required.

The natural comparison for the schemes proposed in this work is with the path conservative schemes for non conservative systems developed by Castro, Pares and coworkers, see the recent review in [39]. In path conservative schemes the contribution of the non conservative products must be split in left going and right going waves at interfaces to account for the correct direction of the fluxes into and outside cells. This requires to take into account some knowledge of the eigenstructure of the matrix of the quasi linear system. As we will see the methods proposed in this work do not need this distinction. A strategy similar to the path conservative Roe scheme by [9] can be found in [17]. Here the path integral is computed using Osher numerical flux, and, as for the Roe flux, a detailed knowledge of the eigenstructure of the flux matrix is needed. Among methods recently proposed for non conservative systems we also mention the entropy stable, time splitting method found in [4]. This method applies to the two layers shallow water system of equations, and it is based on a time splitting which ensures that the contribution of the non conservative products is circumvented. The scheme proposed in that work is very fast, and it satisfies non linear stability through an entropy condition. However the time splitting used simplifies the system up to the point that spurious solutions are observed.

The organization of the paper is as follows: in Section 2 the strategy to extend central schemes on staggered grids to general systems of the form (1.6) is introduced and the main theoretical and practical difficulties are also discussed. In Section 3 the suitable notation for the precise description of the algorithms is set and two different strategies to compute the RK fluxes are introduced. In Section 4 the methods are applied to systems of the form (1.4) and (1.5). The particular cases of the one and the two-layer shallow water models are singled out and we show how to enforce the well-balanced property for these particular cases. Several numerical 1D and 2D tests are presented in Section 5 to check the properties and the accuracy of the numerical methods here introduced. Finally, some concluding remarks are drawn.

2 Central Runge-Kutta methods for nonconservative systems: main idea and difficulties

We consider general systems of the form

$$w_t + A(w)w_x = 0, \quad x \in \mathbb{R},\ t > 0, \tag{2.1}$$

where $w \in \mathbb{R}^m$, and $A(w)$ is a smooth locally bounded matrix-valued function from $\mathbb{R}^m$ to $\mathbb{R}^{m\times m}$. The system is supposed to be strictly hyperbolic and the characteristic fields $r_i(w)$, $i = 1, \dots, m$, are supposed to be either genuinely nonlinear:

$$\nabla\lambda_i(w) \cdot r_i(w) \neq 0, \quad \forall w,$$

or linearly degenerate:

$$\nabla\lambda_i(w) \cdot r_i(w) = 0, \quad \forall\, w.$$

Here, $\lambda_1(w), \dots, \lambda_m(w)$ represent the real eigenvalues of $A(w)$ (in increasing order) and $r_1(w), \dots, r_m(w)$ is a set of associated eigenvectors.

A first important difficulty comes from the definition of weak solution, as the framework of the theory of distributions cannot be applied to define them when the system cannot be written in divergence form. Under some hypotheses of regularity for A, the theory introduced by Dal Maso, LeFloch, and Murat [13] allows one to define the nonconservative product $A(w)w_x$ as a bounded measure for functions w with bounded variation, which may have step-like singularities, provided a family of Lipschitz continuous paths, $\Phi(s; w_L, w_R)$, $s \in [0, 1]$, is prescribed, which must satisfy certain regularity and compatibility conditions, in particular

$$\Phi(0; w_L, w_R) = w_L, \qquad \Phi(1; w_L, w_R) = w_R, \qquad \Phi(s; w, w) = w. \tag{2.2}$$

The interested reader is addressed to [13] for a rigourous and complete presentation of this theory. Here, the family of paths will be just understood as a tool to give a sense to integrals of the form:

$$\int_a^b A(v(x))v_x(x)\,dx,$$

for functions v with jump discontinuities. More precisely, given a bounded variation function $v:[a,b]\to\mathbb{R}^m$, we define:

$$\int\!\!\!\!\!\!-_a^b A(v(x))v_x(x)\,dx = \int_a^b A(v(x))v_x(x)\,dx + \sum_n \int_0^1 A(\Phi(s;v_n^-,v_n^+))\frac{\partial\Phi}{\partial s}(s;v_n^-,v_n^+)\,ds. \tag{2.3}$$

In this definition, v_n^- and v_n^+ represent, respectively, the limits of v to the left and right of its n-th discontinuity (remember that the set of discontinuities of a bounded variation function is countable). Observe that, in (2.3), the family of paths has been used to determine the Dirac measures placed at the discontinuities of v, and the first term on the RHS is the integral computed in regions of smoothness of v, in the usual sense. In the following with the dashed integral we will always consider the operator defined in (2.3).

Notice that the meaning of the nonconservative products and thus the concept of weak solution has to be assigned together with the system of equations, and its initial/boundary conditions. A concept of entropy is also necessary to select the relevant physical solutions as it occurs in systems of conservation laws. Thus we consider an entropy pair (η,g), i.e. a pair of regular functions from $\mathbb{R}^m$ to $\mathbb{R}$, η being convex, such that

$$\nabla g(w) = \nabla\eta(w)\cdot A(w), \quad \forall\, w\in\mathbb{R}^m.$$

A weak solution is said to be an entropy solution if it satisfies the inequality

$$\eta(w)_t + g(w)_x \le 0 \tag{2.4}$$

in the distributional sense.

We are now ready to extend the construction of CRK finite volume schemes based on staggered grids [40] to the case of hyperbolic systems with nonconservative products.

Let us suppose that some approximations $\bar w_j^n$ of the cell averages of the sought weak solution are known at the time $t^n=n\Delta t$ and that a high order essentially non-oscillatory reconstruction operator is applied to these cell averages to obtain a piecewise smooth approximation of the solution at the time t^n:

$$w^n(x) = \sum_j R_j^n(x)\chi_{I_j}(x), \quad \forall x.$$

The initial value problem:

$$\begin{cases} \tilde w_t + A(\tilde w)\tilde w_x = 0, \quad x\in\mathbb{R},\ t\in(t^n,t^{n+1}], \\ \\ \tilde w(x,t^n) = w^n(x), \quad x\in\mathbb{R}, \end{cases} \tag{2.5}$$

is then considered. The averages of its solution at the staggered grid satisfy now the initial value problem:

$$\begin{cases} \bar w'_{j+1/2}(t) = -\dfrac{1}{\Delta x}\displaystyle\int\!\!\!\!\!\!-_{x_j}^{x_{j+1}} A(\tilde w(x,t))\tilde w_x(x,t)\,dx, \quad t\in(t^n,t^{n+1}) \\ \\ \bar w_{j+1/2}(t^n) = \bar w_{j+1/2}^n, \end{cases} \tag{2.6}$$

where

$$\bar w_{j+1/2}^n = \frac{1}{\Delta x}\int_{x_j}^{x_{j+1}} w^n(x)\,dx = \frac{1}{\Delta x}\int_{x_j}^{x_{j+1/2}} R_j^n(x)\,dx + \frac{1}{\Delta x}\int_{x_{j+1/2}}^{x_{j+1}} R_{j+1}^n(x)\,dx. \tag{2.7}$$

(2.6) is satisfied in the weak sense:

$$\int_{t^n}^{t^{n+1}} \varphi'(t)\,\bar{w}_{j+1/2}(t)\,dt - \frac{1}{\Delta x}\int_{t^n}^{t^{n+1}} \fint_{x_j}^{x_{j+1}} \varphi(t)\,A(\tilde{w}(x,t))\tilde{w}_x(x,t)\,dx\,dt$$
$$+\varphi(t^n)\,\bar{w}^n_{j+1/2} = 0, \quad \forall \varphi \in \mathcal{C}^1_0\big[t^n, t^{n+1}\big),$$

where $\mathcal{C}^1_0\big[t^n, t^{n+1}\big)$ represents the space of $\mathcal{C}^1$ functions $\varphi : [t^n, t^{n+1}) \mapsto \mathbb{R}$ with compact support.

Since the reconstruction is only discontinuous at the intercells, if Δt is small enough the resulting Riemann fan will remain within (x_j, x_{j+1}) and thus the solution of (2.5) will remain smooth at the boundaries of the staggered cell. As a consequence no exact or approximate Riemann solver is required to compute and split Dirac masses located at the extrema of the interval, as it is done in *path-conservative* numerical methods: see [38]. In these methods, the equations satisfied by the cell averages of the solution of (2.5) which are now

$$\begin{cases} \bar{w}'_j(t) = -\dfrac{1}{\Delta x}\fint_{x_{j-1/2}}^{x_{j+1/2}} A(\tilde{w}(x,t))\tilde{w}_x(x,t)\,dx, \quad t \in (t^n, t^{n+1}), \\ \\ \bar{w}_j(t^n) = \bar{w}^n_j, \end{cases} \tag{2.8}$$

are approached by:

$$\begin{cases} \bar{w}'_j(t) = -\dfrac{1}{\Delta x}\left(D^+_{i-1/2}(t) + D^-_{i+1/2}(t) + \displaystyle\int_{x_{j-1/2}}^{x_{j+1/2}} A(R^t_j(x))\partial_x R^t_j(x)\,dx\right), \quad t \in (t^n, t^{n+1}), \\ \\ \bar{w}_j(t^n) = \bar{w}^n_j, \end{cases} \tag{2.9}$$

where

$$w^t(x) = \sum_j R^t_j(x)\chi_{I_j}(x), \quad \forall x,$$

is the piecewise smooth function obtained by applying the reconstruction operator to the vector $\{\bar{w}_j(t)\}$;

$$D^\pm_{j+1/2}(t) = D^\pm(w^{t,-}_{j+1/2}, w^{t,+}_{j+1/2}),$$

where

$$w^{t,-}_{j+1/2} = \lim_{x \to x^-_{j+1/2}} R^t_j(x), \quad w^{t,+}_{j+1/2} = \lim_{x \to x^+_{j+1/2}} R^t_{j+1}(x),$$

and $D^\pm$ are two functions satisfying

$$D^-(w_L, w_R) + D^+(w_L, w_R) = \int_0^1 A(\Phi(s; w_L, w_R))\frac{\partial \Phi}{\partial s}(s; w_L, w_R)\,ds, \quad \forall w_L, w_R \in \mathbb{R}^m,$$

$$D^\pm(w, w) = 0, \quad \forall w \in \mathbb{R}^m.$$

The definition of the functions $D^\pm$, which are used to split the Dirac masses at the boundaries of the cells, depends on the method. An adequate choice of these two functions requires some knowledge of the Riemann problems to ensure stability. For instance, in Roe methods

$$D^\pm(w_L, w_R) = A^\pm(w_L, w_R)\cdot(w_R - w_L),$$

where $A(w_L, w_R)$ is a matrix with m different real eingenvalues satisfying the generalized Roe property (see [48]):

$$A(w_L, w_R)\cdot(w_R - w_L) = \int_0^1 A(\Phi(s; w_L, w_R))\frac{\partial \Phi}{\partial s}(s; w_L, w_R)\,ds,$$

and $A^{\pm}(w_L, w_R)$ are the positive and negative part of $A(w_L, w_R)$ in the usual sense. Note that the calculations of the positive and negative part requires an explicit knowledge of the eigenstructure of the matrix.

Coming back to the central approach based on staggered grids, one of its main advantages is that no information concerning the Riemann problems is needed to design the numerical method: to advance in time, a Runge-Kutta scheme is applied to (2.6). The Runge-Kutta fluxes will be obtained by computing the dashed integrals in the RHS of (2.6) at the stage values. While at the first stage (corresponding to $t = t^n$) the value of the dashed integral can be explicitly calculated by:

$$\begin{aligned}\fint_{x_j}^{x_{j+1}} A(\tilde{w}(x,t^n))\tilde{w}_x(x,t^n)\,dx &= \int_{x_j}^{x_{j+1/2}} A(R_j^n(x))\,\partial_x R_j^n(x)\,dx \\ &+ \int_0^1 A(\Phi(s; w_{j+1/2}^{n,-}, w_{j+1/2}^{n,+})\frac{\partial \Phi}{\partial s}(s; w_{j+1/2}^{n,-}, w_{j+1/2}^{n,+}))\,ds \\ &+ \int_{x_{j+1/2}}^{x_{j+1}} A(R_{j+1}^n(x))\partial_x R_{j+1}^n(x)\,dx, \end{aligned} \tag{2.10}$$

(where $w_{j+1/2}^{n,\pm}$ represent the reconstructed states at the intercells), at the stages corresponding to times $t \in (t^n, t^{n+1}]$ an explicit knowledge (or at least an approximation) of $\tilde{w}(\cdot, t)$ in $[x_j, x_{j+1}]$ is needed to compute this dashed integral. This is the main difference with conservative problems, for which this integral can be written as flux differences, so that only the solutions at x_j and x_{j+1} have to be known (or approached). As solving exactly (2.6) is completely out of scope, we will look for suitable approximations. In Section 3 two different strategies to compute the RK fluxes leading to two different versions of the method will be proposed.

Before describing in detail these two versions, we wish to address two theoretical difficulties linked to the discretization of nonconservative systems using families of paths. The first difficulty is related to the choice of the family. Once a family of paths has been chosen, the jump conditions are

$$\xi \cdot (w^+ - w^-) = \int_0^1 A(\Phi(s; w^-, w^+))\frac{\partial \Phi}{\partial s}(s; w^-, w^+)\,ds, \tag{2.11}$$

where ξ is the speed of propagation of the discontinuity, and w^- and w^+ are the left and right limits of the solution at the discontinuity. Therefore, the speed of propagation of shocks, and thus the definition of the weak solutions, explicitly depends on the choice of the family of paths. The crucial question is thus how to choose the 'good' family of paths. The key point is that, in general, first order hyperbolic models are obtained by neglecting some higher order terms whose effects are supposed to be small. Therefore, discontinuities appearing in weak solutions are supposed to be the limits of travelling waves of the regularized system as the high order terms tend to 0. While in systems of conservation laws the jump conditions given by this passage to the limit are the classical Rankine-Hugoniot conditions

$$\xi[u] = [f(u)], \tag{2.12}$$

independently of the particular form of the vanishing high order terms, in nonconservative systems the jump conditions and thus the definition of weak solutions of the hyperbolic system do depend on their particular form. Therefore, the family of paths to be chosen has to be such that the jump conditions (2.11) coincide with the ones obtained from the travelling waves of the regularised problems by passing to the limit. If, for instance, the hyperbolic model has been obtained by neglecting a diffusion term, a good family of paths has to be consistent with the viscous profiles of the parabolic problem with vanishing viscosity: see [30] for a review. Moreover, it has also to be consistent with the integral curves of the characteristic fields and the solutions of the Riemann problems: see [29]. Therefore, the computation of a good family of paths may require both the computation of viscous profiles and the solution of Riemann problems, what may be very costly and/or very difficult. Here, we propose to use the family of straight segments:

$$\Phi(s; w_L, w_R) = w_L + s(w_R - w_L), \tag{2.13}$$

as, at least for smooth flows or weak shocks, this choice will give first order approximation of the actual path, since for a general Lipshitz continuous Φ:

$$\Phi(s; w_L, w_R) = w_L + s(w_R - w_L) + o(||w_R - w_L||),$$

The second main difficulty is related to the convergence of the numerical solutions: even if the correct family of paths is chosen, the limits of the numerical solutions may be weak solutions corresponding to a different choice of paths from the prescribed one. In fact, whenever a numerical scheme having some numerical viscosity is applied to a nonconservative system, the shocks appearing in the numerical solutions are consistent with the viscous profiles induced by the numerical viscosity of the scheme. Since these viscous terms are different in general from the physical ones they may lead to different jump conditions. This fact, which is strongly related to the difficulties of convergence appearing when a nonconservative method is applied to a system of conservation laws (see [21]), has been analyzed in [8] for nonconservative systems when a path-conservative method is applied. Recently, a new example illustrating the difficulties discussed in [21] has been studied in [1]: the authors show that, as expected, the difficulties of convergence are still present when a system of conservation laws is discretized by means of a nonconservative method which is path-conservative with respect to a nonconservative reformulation of the system.

Therefore, with the proposed ansatz it cannot be expected to obtain numerical methods whose solutions converge to the physical weak solutions for general nonconservative systems. Nevertheless, what can be expected is to obtain stable, robust, easy-to-implement numerical methods such that:

- For systems of balance laws (1.4) with smooth σ the limits of the numerical solutions satisfy the physical jump conditions: see [32].
- For nonconservative systems in which the nonconservative products vanish across shocks and only act on contact discontinuities, the limits of the numerical solutions also satisfy the physical jump conditions. This is the case for systems coupling some balance laws with some transport equations (as it happens in turbidity currents models) or for some two-phase fluids models, as the Baër-Nunziato one: see [5], [31], [15] and the references therein.
- For general nonconservative systems the limit of the numerical solution, for the mesh width going to zero, may be a weak solution consistent with the viscous profiles related to the numerical viscosity and not to the physical one. But the difference between these two weak solutions is expected to be small at least for small amplitude shocks: the numerical Hugoniot curves of the states that can be linked by an entropy shock to a given state are expected to be at least first order approximations of the exact Hugoniot curves: see [8].
- Finally, as it will be proven below, paths of the form (2.13) preserve steady states for many systems, as shallow water models.

Let us discuss the relation between the well-balanced property and the choice of paths. For this purpose, let us suppose that $w(x)$ is a smooth stationary solution of (2.1), i.e.

$$A(w(x))w_x = 0, \quad \forall x. \tag{2.14}$$

Observe that this equation can be interpreted as follows: for every x such that $w_x(x) \neq 0$, 0 is an eigenvalue of $A(w(x))$ and $w_x(x)$ is an associated eigenvector. Therefore, if $w_x(x)$ only vanishes in some isolated points, the parametric curve

$$x \to w(x) \in \mathbb{R}^m \tag{2.15}$$

lies on an integral curve Γ of a characteristic field whose corresponding eigenvalue takes always the value 0. Therefore, the characteristic field has to be linearly degenerate. Let us suppose that the chosen family of paths has the following property: if two states w_L and w_R belong to Γ, then

$$\Phi(s; w_L, w_R) \in \Gamma, \quad \forall s \in [0, 1], \tag{2.16}$$

and thus

$$A(\Phi(s; w_L, w_R))\partial_s \Phi(s; w_L, w_R) = 0, \quad \forall s \in [0,1], \ \forall w_L, w_R \in \Gamma. \tag{2.17}$$

If in particular the family of straight segments has been chosen, (2.16) is satisfied for all the stationary solutions such that the parametric curve (2.15) lies on a straight line. This is the case for water at rest solutions for both the one and the two-layer shallow water systems: see Section 4.

Let us also suppose that the reconstruction operator R has the following property: given a stationary solution w taking values on Γ, then

$$Rw(x) \in \Gamma, \quad \forall x, \tag{2.18}$$

being Rw the piecewise smooth function obtained by applying the reconstruction operator to the cell averages of w. Therefore:

$$A(Rw(x))\partial_x Rw(x) = 0, \quad \forall x. \tag{2.19}$$

Notice that the reconstruction operator produces piecewise smooth functions whose restrictions at the cells, in our case, are polynomials or hyperbolas, so that (2.18) is not expected to be satisfied in general, but it is possible to design reconstruction operators on the basis of standard ones that satisfy this property either exactly or numerically with a much higher accuracy than the order of the method: see [10], [36], [42], [43] for some recent results. Nevertheless, for the shallow water systems considered here, the integral curves Γ corresponding to water at rest solutions are straight lines, and (2.19) can be easily obtained with a standard operator just by reconstructing along equilibrium variables.

If (2.17), (2.19) are satisfied and a stationary solution w taking values in Γ is chosen as initial condition, the solution of (2.5) for $n = 0$ is $\tilde{w}(x,t) = w(x)$ and thus, for any $t \in [t^n, t^{n+1}]$:

$$\begin{aligned}
&\fint_{x_j}^{x_{j+1}} A(\tilde{w}(x,t))\tilde{w}_x(x,t)\,dx = \int_{x_j}^{x_{j+1/2}} A(R_j(x))\,\partial_x R_j(x)\,dx \\
&+ \int_0^1 A(\Phi(s; w^-_{j+1/2}, w^+_{j+1/2}))\frac{\partial \Phi}{\partial s}(s; w^-_{j+1/2}, w^+_{j+1/2}))\,ds \\
&+ \int_{x_{j+1/2}}^{x_{j+1}} A(R_{j+1}(x))\partial_x R_{j+1}(x)\,dx,
\end{aligned} \tag{2.20}$$

where:

$$w^+_{j-1/2} = \lim_{x \to x^+_{j-1/2}} R_j(x), \quad w^-_{j+1/2} = \lim_{x \to x^-_{j+1/2}} R_j(x),$$

are the reconstructed states which also belong to Γ by (2.18). Now the three integrals in (2.20) vanish because of (2.17) and (2.19). Therefore all the RK fluxes also vanish and thus

$$\bar{w}^{n+1}_{j+1/2} = \bar{w}^n_{j+1/2}. \tag{2.21}$$

However this equality is not enough to ensure the well-balanced property: the reconstruction step at the staggered grid should be performed in such a way that

$$\bar{w}^{n+2}_j = \bar{w}^n_j. \tag{2.22}$$

We will show in Subsections 4.1 and 4.2 that, to obtain (2.22) for water at rest solutions, it is enough again to reconstruct along equilibrium variables.

3 Central Runge-Kutta methods for nonconservative systems: detailed description

Before giving a precise description of Central Runge-Kutta methods for nonconservative systems, we need to set a suitable notation for Runge-Kutta schemes applied to initial value problems. Therefore let:

$$\begin{cases} y' = g(y), \\ y(t_0) = y_0. \end{cases}$$

Let us apply to the initial value problem above an explicit Runge-Kutta scheme with ν stages to obtain the numerical solution at time $n\Delta t$ as:

$$y^{n+1} = y^n + \Delta t \sum_{i=1}^{\nu} b_i K^{(i)}.$$

The $K^{(i)}$ are called *Runge-Kutta fluxes* and are defined by:

$$K^{(i)} = g(y^{(i)}) \quad i = 1, \cdots, \nu,$$

where the $y^{(i)}$ will be called *stage values*, and, for an explicit scheme, are given by:

$$y^{(i)} = y^n + \Delta t \sum_{l=1}^{i-1} a_{i,l} K^{(l)}, \quad i = 1, \cdots, \nu.$$

The matrix $\mathcal{A} = (a_{i,l})$, and the vector $b = (b_i)$ uniquely define the RK scheme. With the present notation, $\mathcal{A}$ is a $\nu \times \nu$ lower triangular matrix, with zero elements on the diagonal.

We will describe now the two versions of our scheme. Both of them require the introduction of an essentially non-oscillatory reconstruction operator, i.e. an operator that, starting from a vector of cell averages $\{\bar{v}\}$, provides a piecewise smooth function of the form:

$$R(x; \{\bar{v}\}) = \sum_j R_j(x; [\bar{v}_{j-k_0}, \ldots, \bar{v}_{j+k_1}]) \chi_{I_j}(x), \tag{3.1}$$

where $\bar{v}_j$ denotes the cell average on the j-th cell; χ_{I_j} is the characteristic function of the interval I_j; k_0, k_1 are two fixed natural numbers; and $R_j(x; [\bar{v}_{j-k_0}, \ldots, \bar{v}_{j+k_1}])$ is a smooth function obtained by using interpolation or approximation techniques from the values at some neighboring cells $I_{j-k_0}, \ldots, I_{j+k_1}$ that constitute the *stencil* of the reconstruction.

Given a function v, we will denote by $\bar{v}_j$ its average at the cell I_j: $\bar{v}_j = \frac{1}{\Delta x} \int_{I_j} v(x)\, dx$, and by Rv the approximation function obtained by applying the reconstruction operator to the vector $\{\bar{v}\}$ collecting all its cell averages, i.e.

$$Rv(x) = R(x, \{\bar{v}\}), \quad \forall x.$$

The reconstruction has to be conservative in the following sense $\overline{R(x; \{\bar{v}\})}_j = \bar{v}_j, \quad \forall j$, and it has to give accurate estimates of the point values and derivatives of smooth functions. More precisely, if v is a smooth function, we want that:

$$v^{\pm}_{j+1/2} = \lim_{x \to x^{\pm}_{j+1/2}} Rv(x) = v(x_{j+1/2}) + O(\Delta x^p), \tag{3.2}$$

and, if $x \in (x_{j-1/2}, x_{j+1/2})$ for some j:

$$Rv(x) = v(x) + O(\Delta x^q), \qquad \partial_x Rv(x) = v'(x) + O(\Delta x^{q-1}). \tag{3.3}$$

$$Rv(x) = v(x) + O(\Delta x^q), \tag{3.4}$$

$$\partial_x Rv(x) = v'(x) + O(\Delta x^{q-1}). \tag{3.5}$$

For most reconstruction operators, as MUSCL, ENO or PHM, $q = p$, while for WENO one can achieve $p = 2q - 1$. Here, only reconstruction operators satisfying $q = p$ will be considered.

Let us suppose that the approximations of the cell averages of the sought solution at time t^n, $\bar{w}^n_j$, have been obtained. Then, in order to evaluate the initial staggered cell average, the reconstruction operator is applied to the vector of cell averages $\{\bar{w}^n\}$. The following notation will be used:

$$w^n(x) = R(x, \{\bar{w}^n\}) = \sum_j R_j(x; [\bar{w}^n_{j-k_0}, \ldots, \bar{w}^n_{j+k_1}]), \quad \forall x. \tag{3.6}$$

If the integrals are exactly computed, the initial staggered cell average is given by (2.7). Otherwise, a quadrature formula has to be chosen on the intervals $[x_j, x_{j+1/2}]$ and $[x_{j+1/2}, x_{j+1}]$ whose nodes and weights will be denoted respectively by

$$x^l_{j+1/4}, \quad x^l_{j+3/4}, \qquad \alpha^l_{j+1/4}, \quad \alpha^l_{j+3/4}, \qquad l = 0, \dots, \mu,$$

Then w^n is evaluated at the nodes of the quadrature rule:

$$w^{l,n}_{j+1/4} = w^n(x^l_{j+1/4}) \qquad w^{l,n}_{j+3/4} = w^n(x^l_{j+3/4}), \qquad l = 0, \dots, \mu. \tag{3.7}$$

In the numerical experiments we will show, the point $x_{j+1/2}$ is a quadrature node on each of the two sub-cells, namely $x_{j+1/2} = x^{\mu}_{j+1/4}$ and $x_{j+1/2} = x^0_{j+3/4}$, and the points x_j and x_{j+1} are also quadrature nodes $x_j = x^0_{j+1/4}$ and $x_{j+1} = x^{\mu}_{j+3/4}$, so in particular:

$$w^{\mu,n}_{j+1/4} = w^{-,n}_{j+1/2}, \qquad w^{0,n}_{j+3/4} = w^{+,n}_{j+1/2}. \tag{3.8}$$

Thus the approximation to (2.7) becomes:

$$\overline{w}^n_{j+1/2} = \sum_{l=0}^{\mu} \left[\alpha^l_{j+1/4}\, w^{l,n}_{j+1/4} + \alpha^l_{j+3/4}\, w^{l,n}_{j+3/4} \right]. \tag{3.9}$$

The new cell averages will be computed by integrating (2.6) with an order p Runge-Kutta scheme:

$$\bar{w}^{n+1}_{j+1/2} = \bar{w}^n_{j+1/2} - \lambda \sum_{i=1}^{\nu} b_i K^{(i)}_{j+1/2}, \tag{3.10}$$

where $\lambda = \frac{\Delta t}{\Delta x}$ and the quantities $K^{(i)}_{j+1/2}$ are the RK fluxes. We describe hereafter two different strategies to evaluate these fluxes.

Version 1.

This version, which follows closely the usual ansatz in central schemes on staggered grids for conservative problems, is targeted on minimazing the points on which the Runge Kutta stage values are computed. To do this, a new reconstruction operator is needed, $\tilde{R}$, which starting from a vector of point values $\{v\}$, provides again a piecewise smooth function of the form:

$$\tilde{R}(x; \{v\}) = \sum_j \tilde{R}_j(x; [v_{j-\tilde{k}_0}, \dots, v_{j+\tilde{k}_1}]) \chi_{I_j}(x), \tag{3.11}$$

where $\tilde{k}_0, \tilde{k}_1$ are two fixed natural numbers and $\tilde{R}_j(x; [v_{j-\tilde{k}_0}, \dots, v_{j+\tilde{k}_1}])$ is again a smooth function obtained by using interpolation or approximation techniques from the values in the stencil.

Given a function v, we will denote by $\tilde{R}v$ the approximation function obtained by applying this new reconstruction operator to the vector $\{v\}$ collecting the point values of v at the center of the cells x_j, i.e.

$$\tilde{R}v(x) = \tilde{R}(x, \{v\}), \quad \forall x.$$

As the reconstruction is calculated on the basis of point values and not cell averages, $\tilde{R}$ does not need to be conservative, but still it has to give accurate estimates of the point values and derivatives of a smooth function v:

$$\tilde{v}^{\pm}_{j+1/2} = \lim_{x \to x^{\pm}_{j+1/2}} \tilde{R}v(x) = v(x_{j+1/2}) + O(\Delta x^p), \tag{3.12}$$

and, if $x \in (x_{j-1/2}, x_{j+1/2})$ for some j:

$$\tilde{R}v(x) = v(x) + O(\Delta x^q), \tag{3.13}$$

$$\partial_x \tilde{R}v(x) = v'(x) + O(\Delta x^{q-1}). \tag{3.14}$$

Note that since $\tilde{R}$ acts across discontinuities, it needs to be a non-oscillatory reconstruction operator.

With these information, we evaluate the stage values, using the PDE in its differential form, as in CRK schemes, see [40]:

For $i = 1, \dots, \nu$:

$$w_j^{(i)} = w^n(x_j) - \Delta t \sum_{l=1}^{i-1} a_{i,l} \hat{K}_j^{(l)}, \tag{3.15}$$

$$\hat{K}_j^{(i)} = A(w_j^{(i)}) \partial_x \tilde{R}^{(i)}(x_j), \tag{3.16}$$

where

$$\tilde{R}^{(1)}(x) = w^n(x) = R(x, \{\bar{w}^n\}), \quad \forall x, \tag{3.17}$$

$$\tilde{R}^{(i)}(x) = \tilde{R}(x; \{w^{(i)}\}) = \sum_j \tilde{R}_j(x; [w_{j-\tilde{k}_0}^{(i)}, \dots, w_{j+\tilde{k}_1}^{(i)}]) \chi_{I_j}(x), \quad \forall x. \tag{3.18}$$

Once this is done, the Runge-Kutta fluxes appearing in (3.10) can be computed as:

$$\begin{aligned} K_{j+1/2}^{(i)} &= \int_{x_j}^{x_{j+1/2}} A(\tilde{R}^{(i)}(x)) \, \partial_x \tilde{R}^{(i)}(x) \, dx + \int_{x_{j+1/2}}^{x_{j+1}} A(\tilde{R}^{(i)}(x)) \partial_x \tilde{R}^{(i)}(x) \, dx \\ &\quad + \int_0^1 A(\Phi(s; \tilde{w}_{j+1/2}^{(i),-}, \tilde{w}_{j+1/2}^{(i),+})) \frac{\partial \Phi}{\partial s}(s; \tilde{w}_{j+1/2}^{(i),-}, \tilde{w}_{j+1/2}^{(i),+}) \, ds, \end{aligned} \tag{3.19}$$

where

$$\tilde{w}_{j+1/2}^{(i),\pm} = \lim_{x \to x_{j+1/2}^{\pm}} \tilde{R}^{(i)}(x). \tag{3.20}$$

In practice, the quadrature formulae are used to compute the RK fluxes:

$$\begin{aligned} K_{j+1/2}^{(i)} &= \sum_{l=0}^{\mu} \left[\alpha_{j+1/4}^l A(w_{j+1/4}^{l,(i)}) \, (w_x)_{j+1/4}^{l,(i)} + \alpha_{j+3/4}^l A(w_{j+3/4}^{l,(i)}) \, (w_x)_{j+3/4}^{l,(i)} \right] \\ &\quad + \int_0^1 A(\Phi(s; \tilde{w}_{j+1/2}^{(i),-}, \tilde{w}_{j+1/2}^{(i),+})) \frac{\partial \Phi}{\partial s}(s; \tilde{w}_{j+1/2}^{(i),-}, \tilde{w}_{j+1/2}^{(i),+}) \, ds, \end{aligned} \tag{3.21}$$

where, for $l = 0, \dots, \mu$, $\gamma = 1/4, 3/4$, $i = 1, \dots, \nu$, $w_{j+\gamma}^{l,(i)} = \tilde{R}^{(i)}(x_{j+\gamma}^l)$, and $(w_x)_{j+\gamma}^{l,(i)} = \partial_x \tilde{R}^{(i)}(x_{j+\gamma}^l)$. This completes the description of Version 1 of the scheme. In this approach, we perform the following steps:

- At the beginning of the time step, we compute a non-oscillatory reconstruction from cell averages, yielding all values of the solution and of its space derivative at all quadrature nodes, and with this information we evaluate the cell average on the staggered cell.
- We evolve the stage values only in the middle of each cell.
- At each stage value, a non-oscillatory reconstruction step from point values is needed to compute all quantities appearing in (3.19).

Version 2.

In this version, which is designed in order to minimize the essentially non-oscillatory reconstruction steps, the solution of (2.5) is approached by:

$$\tilde{w}(x,t) \cong \sum_j \tilde{w}_j(x,t) \chi_{I_j}(x), \quad x \in \mathbb{R}, \ t \in [t^n, t^{n+1}], \tag{3.22}$$

where $\tilde{w}_j$ is the solution of the initial value problem

$$\begin{cases} \partial_t \tilde{w}_j + A(\tilde{w}_j)\partial_x \tilde{w}_j = 0, \quad x \in \mathbb{R},\ t \in (t^n, t^{n+1}], \\ \tilde{w}_j(x, t^n) = R_j^n(x), \quad x \in \mathbb{R}, \end{cases} \tag{3.23}$$

where we assume that the reconstruction functions at the cells, R_j^n, have a natural smooth extension to the whole real line, as it happens in practice. If Δt is small enough, the solution $\tilde{w}_j$ of the problems (3.23) is expected to remain smooth in $[x_j, x_{j+1}] \times [t^n, t^{n+1}]$ so that (3.22) provides a piecewise smooth approximation of the solution of (2.5) whose discontinuities are placed at the intercells and whose restrictions to the cells are classical solutions: a similar approach has been followed in [14], [15] in the context of ADER or Garlerkin-discontinuous methods.

The initial staggered cell value is computed again by (3.9), but now *all* the reconstructed values of the solution at the quadrature nodes (3.7) are evolved in time by using again the differential form of the PDE (3.23):

For $l = 0, \ldots, \mu$, $\gamma = 1/4, 3/4$, $i = 1, \ldots, \nu$, $\forall j$:

$$w_{j+\gamma}^{l,(i)} = w_{j+\gamma}^{l,n} - \Delta t \sum_{k=1}^{i-1} a_{i,k} \hat{K}_{j+\gamma}^{l,(k)}, \tag{3.24}$$

$$\hat{K}_{j+\gamma}^{l,(i)} = A(w_{j+\gamma}^{l,(i)})(w_x)_{j+\gamma}^{l,(i)}, \tag{3.25}$$

where

$$w_{j+\gamma}^{l,n} = R_j^n(x_{j+\gamma}^l), \qquad (w_x)_{j+\gamma}^{l,(1)} = \partial_x R_j^n(x_{j+\gamma}^l), \qquad (w_x)_{j+\gamma}^{l,(i)} = \partial_x P_{j+\gamma}^{(i)}(x_{j+\gamma}^l).$$

Here, $P_{j+\gamma}^{(i)}$ is obtained by interpolating the data $(x_{j+\gamma}^0, w_{j+\gamma}^{0,(i)}), \ldots, (x_{j+\gamma}^\mu, w_{j+\gamma}^{\mu,(i)})$. In order to achieve order p, at least $p+1$ data are required, so that $\mu \geq p$.

At this point, the RK fluxes simplify using (3.25) and reduce to:

$$\begin{aligned} K_{j+1/2}^{(i)} &= \sum_{l=0}^{\mu} \left[\alpha_{j+1/4}^l \hat{K}_{j+1/4}^{l,(i)} + \alpha_{j+3/4}^l \hat{K}_{j+3/4}^{l,(i)} \right] \\ &\quad + \int_0^1 A(\Phi(s; \tilde{w}_{j+1/2}^{(i),-}, \tilde{w}_{j+1/2}^{(i),+})) \frac{\partial \Phi}{\partial s}(s; \tilde{w}_{j+1/2}^{(i),-}, \tilde{w}_{j+1/2}^{(i),+}))\, ds. \end{aligned} \tag{3.26}$$

Here the data $\tilde{w}_{j+1/2}^{(i),\pm}$ are computed from eq. (3.8). This completes the description of Version 2 of the scheme. In this case, we perform the following tasks:

- At the beginning of the time step, we compute a non-oscillatory reconstruction from cell averages, yielding all values of the solution and of its space derivative at all quadrature nodes, and the cell average on the staggered cell.
- We evolve the stage values in each quadrature node.
- At each stage value, a local and simple polynomial interpolation is needed to evaluate w and its derivative at each quadrature node.

Notice that this strategy entails a significant increase in the number of points in which the system in differential form is solved by means of the RK method. But, on the other hand, a standard interpolation operator is used at every stage so that no regularity estimates or non-oscillatory techniques are required. In fact, in all the numerical tests shown in Section 5 the second strategy leads to algorithms which are less costly in terms of CPU time.

Once the approximation at time t^{n+1} has been obtained, the next step consists in applying the Runge-Kutta scheme to the equation

$$\bar{w}_j' = -\frac{1}{\Delta x}\fint_{x_{j-1/2}}^{x_{j+1/2}} A(w(x,t))w_x(x,t)\,dx. \tag{3.27}$$

to obtain the new cell averages $\bar{w}_j^{n+2}$, starting from the cell values $\bar{w}_{j+1/2}^{n+1}$ on the unstaggered grid.

Although in the general presentation of the methods the time step has been supposed to be constant for simplicity, in practice a CFL-condition is imposed: if we define

$$\mathrm{CFL} = \max_j \left\{ \left|\lambda_{j,i}^n\right|, \quad i = 1,\dots,m \right\} \frac{\Delta t}{\Delta x}, \tag{3.28}$$

where $\lambda_{j,i}^n$, $i = 1,\dots,m$ are the eigenvalues of $A(\bar{w}_j^n)$ (or some adequate approximations), then the value of the parameter CFL belonging to the interval $(0, 1/2]$ is fixed, and Δt varies accordingly.

In Section 5 the reconstruction operators, the quadrature formulae, and the specific values of the parameters adopted here will be reported.

4 A particular case

Let us consider the particular case (1.5) This system can be considered as a particular case of (2.1) where w and $A(w)$ are given by (1.7).

In order to apply the CRK scheme to this problem, the cell averages of σ are calculated both at the initial and the staggered grids at the beginning:

$$\bar{\sigma}_j = \frac{1}{h}\int_{x_{j-1/2}}^{x_{j+1/2}} \sigma(x)\,dx, \tag{4.1}$$

$$\bar{\sigma}_{j+1/2} = \frac{1}{h}\int_{x_j}^{x_{j+1}} \sigma(x)\,dx, \tag{4.2}$$

as well as their reconstructions at both grids:

$$R\sigma(x) = \sum_j R(x;[\bar{\sigma}_{j-k_0},\dots,\bar{\sigma}_{j+k_1}])\chi_{I_j}(x), \tag{4.3}$$

$$R^*\sigma(x) = \sum_j R(x;[\bar{\sigma}_{j+1/2-k_0},\dots,\bar{\sigma}_{j+1/2+k_1}])\chi_{I_{j+1/2}}(x). \tag{4.4}$$

The corresponding reconstructed states at the interfaces will be denoted by $\sigma_{j+1/2}^{\pm}$ and $\sigma_j^{\pm}$. These averages and reconstructions will not be updated during the calculations.

For the sake of shortness, only the details of Version 1 will be described: the expression of the algorithm corresponding to Version 2 is similar. By taking into account the definition of w and $A(w)$, the numerical scheme can be written as follows:

$$\bar{u}_{j+1/2}^{n+1} = \bar{u}_{j+1/2}^n - \lambda\sum_{i=1}^{\nu} b_i K_{j+1/2}^{(i)}, \tag{4.5}$$

where now $K_{j+1/2}^{(i)}$ approximates the forcing term of the equation, namely

$$K_{j+1/2}^{(i)} \simeq \fint_{x_j}^{x_{j+1}} \left[\partial_x f(u^{(i)}) - B(u^{(i)})\partial_x u^{(i)} - S(u^{(i)})\partial_x\sigma\right] \tag{4.6}$$

The following notation will be used:

$$\Phi(s;w_L,w_R) = \begin{bmatrix} \Phi_u(s;w_L,w_R) \\ \Phi_\sigma(s;w_L,w_R) \end{bmatrix},$$

$$u^n(x) = R(x;\{\bar{u}^n\}), \quad \forall x,$$
$$\tilde{R}^{(1)}(x) = R(x;\{\bar{u}^n\}), \quad \tilde{R}^{(i)}(x) = \tilde{R}(x;\{u^{(i)}\}), \quad i = 2,\dots,\nu, \quad \forall x,$$

and the reconstructions R and $\tilde{R}$ have been defined in (3.1) and (3.11). Finally:

$$\tilde{w}^{(i),\pm}_{j+1/2} = \begin{bmatrix} \tilde{u}^{(i),\pm}_{j+1/2} \\ \sigma^{\pm}_{j+1/2} \end{bmatrix},$$

$\{\tilde{u}^{(i),\pm}_{j+1/2}\}$ being the reconstructed states corresponding to the vector of stage values $\{u^{(i)}\}$. These states are calculated now as follows:

$$u^{(i)}_j = u^n(x_j) - \Delta t \sum_{l=1}^{i-1} a_{i,l} \hat{K}^{(l)}_j, \qquad i = 1,\cdots,\nu, \tag{4.7}$$

with the Runge-Kutta fluxes:

$$\hat{K}^{(l)}_j = \left(\nabla f(u^{(l)}_j) - B(u^{(l)}_j)\right) \partial_x \tilde{R}^{(l)}_j(x_j) - S(\tilde{u}^{(l)}_j)\, \partial_x R\sigma_j(x_j), \quad l = 1,\cdots,\nu. \tag{4.8}$$

We exploit the fact that part of the system is in conservative form. Thus some straightforward calculations allow us to rewrite the RK fluxes of the numerical solution as follows:

$$\begin{aligned} K^{(i)}_{j+1/2} &= f(u^{(i)}_{j+1}) - f(u^{(i)}_j) \\ &- \int_{x_j}^{x_{j+1/2}} B(\tilde{R}^{(i)}(x))\, \partial_x \tilde{R}^{(i)}(x)\, dx - \int_{x_{j+1/2}}^{x_{j+1}} B(\tilde{R}^{(i)}(x)) \partial_x \tilde{R}^{(i)}(x)\, dx \\ &- \int_{x_j}^{x_{j+1/2}} S(\tilde{R}^{(i)}(x))\, \partial_x R\sigma(x)\, dx - \int_{x_{j+1/2}}^{x_{j+1}} S(\tilde{R}^{(i)}(x)) \partial_x R\sigma(x)\, dx \\ &- \int_0^1 B(\Phi_u(s;\tilde{w}^{(i),-}_{j+1/2}, \tilde{w}^{(i),+}_{j+1/2})) \frac{\partial \Phi_u}{\partial s}(s;\tilde{w}^{(i),-}_{j+1/2}, \tilde{w}^{(i),+}_{j+1/2})\, ds \\ &- \int_0^1 S(\Phi_u(s;\tilde{w}^{(i),-}_{j+1/2}, \tilde{w}^{(i),+}_{j+1/2})) \frac{\partial \Phi_\sigma}{\partial s}(s;\tilde{w}^{(i),-}_{j+1/2}, \tilde{w}^{(i),+}_{j+1/2})\, ds, \end{aligned} \tag{4.9}$$

This expression makes it apparent that the method reduces to the conservative CRK method whenever the source and nonconservative terms vanish. This is in particular the case for the equations of the system that have the form of a conservation law.

Although the expression (4.9) is equivalent to (3.19), when the integrals are computed exactly, they lead to different schemes when numerical integration is applied, unless the chosen quadrature formula is exact for all the integrals containing the Jacobian of the flux function. When the reconstruction functions are polynomial, it is enough to choose an adequate quadrature formula, but if they are hyperbolas (as it is the case for the third order reconstruction operator considered in Section 5), it is not trivial to find such a formula. In that case, the expression (4.9) seems to be more adequate a priori, as it stills reduces to the conservative CRK method when the source and the nonconservative terms vanish. Nevertheless, if this expression is used, the well-balanced properties of the method with exact integration may be lost. In effect, let us suppose that the family of paths satisfies (2.16) for a certain integral characteristic curve Γ of the null eigenvalue. Then (2.17) can be written in this case as follows:

$$\begin{aligned} \nabla f(\Phi_u(s;w_L,w_R)) \frac{\partial \Phi_u}{\partial s}(s;w_L,w_R) - B(\Phi_u(s;w_L,w_R)) \frac{\partial \Phi_u}{\partial s}(s;w_L,w_R) \\ - S(\Phi_u(s;w_L,w_R)) \frac{\partial \Phi_\sigma}{\partial s}(s;w_L,w_R) = 0, \quad \forall s \in [0,1],\ w_L, w_R \in \Gamma. \end{aligned} \tag{4.10}$$

Let us also suppose that the reconstruction operator R and $\tilde{R}$ are well-balanced for Γ. In this case, property (2.19) writes as follows:

$$\nabla f(Ru(x))\partial_x Ru(x) - B(Ru(x))\partial_x Ru(x) - S(Ru(x))\partial_x R\sigma(x) = 0, \tag{4.11}$$

for every $x \in (x_{j-1/2}, x_{j+1/2})$ for some j. The expression of the well-balanced property for $\tilde{R}$ is analogous.

If all of these properties are satisfied, it can be easily checked that the method with RK fluxes given by (3.19) either with exact or numerical integration is well-balanced for stationary solutions taking values in Γ. But this is not the case in general if the expression of the RK fluxes (4.9) is chosen. Therefore, a compromise between the two possible writings of the flux term is needed in order to have both the well-balanced and the conservation property independently of the quadrature formula. We show hereafter how such a compromise can be found for the one and the two-layer shallow water models.

4.1 Shallow water equations

The shallow water model considered here is the particular case of (1.5) corresponding to the choices $m = 2$, $B = 0$, $\sigma = H$,

$$u = \begin{pmatrix} h \\ q \end{pmatrix}, \quad f(u) = \begin{pmatrix} q \\ \dfrac{q^2}{h} + \dfrac{g}{2}h^2 \end{pmatrix}, \quad S(u) = \begin{pmatrix} 0 \\ gh \end{pmatrix},$$

where $q(x,t)$ and $h(x,t)$ represent the mass-flow and the water thickness, respectively; g, the acceleration due to gravity; $H(x)$, the depth measured from a fixed level of reference; and $\eta = h - H$ is the free surface elevation: see Figure 1.

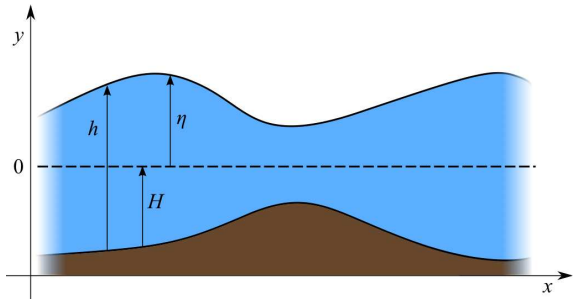

Figure 1: Shallow water model.

The eigenvalues of this system are: $\lambda_1 = v - c$, $\lambda_2 = v + c$, where $v = q/h$ represents the averaged velocity along the vertical direction and $c = \sqrt{gh}$. A state u is said to be supercritical, critical o subcritical if $F_r > 1$, $F_r = 1$, or $F_r < 1$ respectively, $F_r = \frac{|v|}{c}$ being the *Froude number*.

The stationary solutions of the system satisfy the equations:

$$q = constant, \qquad h + \frac{q^2}{2gh^2} - H = constant. \tag{4.12}$$

In the particular case $q = 0$ these curves are straight lines in h, q, H space, and they correspond to water at rest solutions:

$$q = 0, \qquad h - H = constant. \tag{4.13}$$

If the family of straight segments (2.13) is chosen, (2.16) is satisfied for the straight lines Γ whose equations are (4.13). In this case, given a pair of states $w_L = [h_L, q_L, H_L]^T$, $w_R = [h_R, q_R, H_R]^T$ that belong to the same curve (4.13), i.e.

$$q_L = q_R = 0, \quad h_L - H_L = h_R - H_R, \tag{4.14}$$

eq. (4.10) reduces to:

$$\begin{cases} q_R - q_L = 0; \\ \\ -\left(\dfrac{\Phi_q(s;W_L,W_R)}{\Phi_h(s;W_L,W_R)}\right)^2 (h_R - h_L) + g\Phi_h(s;W_L,W_R)(h_R - H_R - (h_L - H_L)) = 0, \quad \forall s \in [0,1], \end{cases} \tag{4.15}$$

which is trivially satisfied due to (4.14) and the fact that $\Phi_q(s;W_L,W_R) = 0, \quad \forall s \in [0,1]$.

On the other hand, a well-balanced reconstruction should satisfy (4.11). If we have a stationary solution taking values on a curve (4.13), the reconstructions Rh, Rq, and RH should satisfy (4.15), which is guaranteed if:

$$\partial_x Rq = 0, \quad gRh(x)(\partial_x Rh(x) - \partial_x RH(x)) = 0, \quad \forall x. \tag{4.16}$$

This property can be easily achieved for any reconstruction able to preserve constant states, if the reconstruction step is performed as follows: given a vector of cell averages $\{\bar{w}\}$ with components $\bar{w}_j = [\bar{h}_j, \bar{q}_j, \bar{H}_j]^T$, the reconstruction operator is first applied to the vector $\{\bar{q}\}$ to obtain Rq and to the vector $\{\bar{\eta}\}$ whose components are $\bar{\eta}_j = \bar{h}_j - \bar{H}_j$ to obtain $R\eta$. Finally, Rh is defined by:

$$Rh = R\eta + RH,$$

recalling that the cell averages of H and its reconstruction RH are computed and fixed at the beginning of the calculations. With this reconstruction procedure, it is clear that (4.16) is satisfied for the reconstructions of stationary solutions taking values on (4.13). The same procedure is applied to the reconstuction operator $\tilde{R}$. This reconstruction procedure may introduce negative values of h even if the reconstruction operator is positivity preserving, as close to wet/dry fronts it may happen that $R\eta(x) < RH(x)$, but suitable techniques can be used to prevent the appearance of negative values of h as in [18].

In order to evaluate the cell averages at the staggered grid, we use first the reconstructions Rq and $R\eta$ to compute $\bar{q}^n_{j+1/2}$, $\bar{\eta}^n_{j+1/2}$, and then we obtain $\bar{h}^n_{j+1/2}$ by:

$$\bar{h}^n_{j+1/2} = \bar{\eta}^n_{j+1/2} + \bar{H}_{j+1/2}.$$

At water at rest equilibria $q = 0$, $\eta = C$, we obtain $\bar{q}^n_{j+1/2} = 0$, $\bar{\eta}^n_{j+1/2} = C$ both when the integrals are computed exactly and when they are computed numerically, and

$$\bar{h}^{n+1}_{j+1/2} = C + \bar{H}_{j+1/2},$$

so that the equilibrium is preserved when passing to the staggered grid. Once the new approximations $\bar{u}^{n+1}_{j+1/2}$ have been obtained, the same procedure is used to compute $\bar{u}^{n+2}_j$.

Concerning the expression of the RK fluxes (3.19), we write as a flux difference all the conservative terms, as in (4.9), except the one related to the pressure in the momentum equation $gh^2/2$. The resulting expression of the two components of the RK fluxes are thus the following:

$$K^{(i)}_{1,j+1/2} = q^{(i)}_{j+1} - q^{(i)}_j, \tag{4.17}$$

$$\begin{aligned} K^{(i)}_{2,j+1/2} = {} & \frac{\left(q^{(i)}_{j+1}\right)^2}{h^{(i)}_{j+1}} - \frac{\left(q^{(i)}_j\right)^2}{h^{(i)}_j} \\ & + \int_{x_j}^{x_{j+1/2}} g\tilde{R}h^{(i)}(x)\left[\partial_x \tilde{R}h^{(i)}(x) - \partial_x RH(x)\right] dx + \int_{x_{j+1/2}}^{x_{j+1}} g\tilde{R}h^{(i)}(x)\left[\partial_x \tilde{R}h^{(i)}(x) - \partial_x RH(x)\right] dx \\ & + \frac{g}{2}\left(\tilde{h}^{(i),-}_{j+1/2} + \tilde{h}^{(i),+}_{j+1/2}\right)\left(\tilde{h}^{(i),+}_{j+1/2} - H^+_{j+1/2} - \tilde{h}^{(i),-}_{j+1/2} + H^-_{j+1/2}\right) \end{aligned} \tag{4.18}$$

Reconstructing along the equilibrium variable η, $\partial_x \tilde{R}h - \partial_x RH = \partial_x \tilde{R}\eta$, and

$$\tilde{h}^{(i),+}_{j+1/2} - H^+_{j+1/2} - \tilde{h}^{(i),-}_{j+1/2} + H^-_{j+1/2} = \eta^{(i),+}_{j+1/2} - \eta^{(i),-}_{j+1/2}$$

Clearly, if $q = 0$ and $\eta = const$, then $\partial_x R\eta(x) = 0$, and $\eta^{(i),+}_{j+1/2} - \eta^{(i),-}_{j+1/2} = 0$. Thus at equilibrium all RK fluxes are zero and the evolution equation for the cell averages reduces to:

$$\bar{u}^{n+1}_{j+1/2} = \bar{u}^{n}_{j+1/2},$$

and this is also the case if a quadrature formula is used in the integral terms, as the integrand vanishes at every node. On the other hand, the way in which the reconstructions at the initial grid are evaluated ensures that $\bar{u}^{n+2}_j = \bar{u}^n_j$.

Therefore, the numerical method is conservative for the mass equation and well-balanced for water at rest solutions, independently of the quadrature formula used to compute the integral terms. It can be also checked that these properties are satisfied by Version 2 if the analogous expressions of the RK fluxes are used.

4.2 The two-layer shallow water system

The two-layer shallow water model (see [11]) is the particular case of (1.5) corresponding to $m = 4$, $\sigma = H$,

$$u(x,t) = \begin{bmatrix} h_1 \\ q_1 \\ h_2 \\ q_2 \end{bmatrix}, \quad F(u) = \begin{bmatrix} q_1 \\ \frac{q_1^2}{h_1} + \frac{g}{2}h_1^2 \\ q_2 \\ \frac{q_2^2}{h_2} + \frac{g}{2}h_2^2 \end{bmatrix}, \quad S(u) \begin{bmatrix} 0 \\ gh_1 \\ 0 \\ gh_2 \end{bmatrix}, \quad B(u) = \begin{bmatrix} 0 & 0 & 0 & 0 \\ 0 & 0 & -gh_1 & 0 \\ 0 & 0 & 0 & 0 \\ -grh_2 & 0 & 0 & 0 \end{bmatrix},$$

where the index 1 refers to the upper layer and the index 2 to the lower one, $q_i(x,t)$ and $h_i(x,t)$ represent respectively the mass-flow and the thickness of the i-th layer, g is the acceleration due to gravity, $H(x)$ represents the depth function measured from a fixed level of reference. Each layer is assumed to have a constant density, ρ_i, $i = 1, 2$ ($\rho_1 < \rho_2$), and

$$r = \frac{\rho_1}{\rho_2}$$

represents the density ratio: see Figure 2.

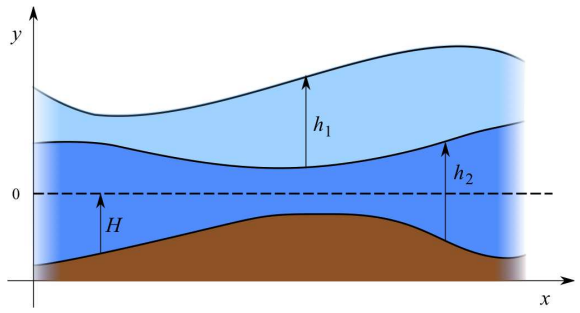

Figure 2: Two-layer shallow water model.

The characteristic equation of the homogeneous system, i.e. the P.D.E. obtained when $H = cons$, is

$$\left(\lambda^2 - 2v_1\lambda + v_1^2 - gh_1\right)\left(\lambda^2 - 2v_2\lambda + v_2^2 - gh_2\right) = rg^2h_1h_2, \tag{4.19}$$

where $v_i = q_i/h_i$ represents the averaged velocity of the i-th layer and $c_i = \sqrt{gh_i}$, $i = 1, 2$.

In the case $r \cong 1$ (which is the situation arising in many geophysical flows) a first-order approximation of the eigenvalues was given in [44]:

$$\lambda^{\pm}_{\text{ext}} \cong \frac{v_1 h_1 + v_2 h_2}{h_1 + h_2} \pm \big(g(h_1 + h_2)\big)^{\frac{1}{2}}, \tag{4.20}$$

$$\lambda^{\pm}_{\text{int}} \cong \frac{v_1 h_2 + v_2 h_1}{h_1 + h_2} \pm \left(g' \frac{h_1 h_2}{(h_1 + h_2)}\Big[1 - \frac{(v_1 - v_2)^2}{g'(h_1 + h_2)}\Big]\right)^{\frac{1}{2}}. \tag{4.21}$$

In the above expression, g' is the *reduced gravity*: $g' = (1 - r)g$. These approximations of the eigenvalues will be used to compute the CFL parameter (3.28). Note that, $\lambda^{\pm}_{\text{int}}$ may become complex, corresponding to the development of shear instabilities. In the present work only the case where $\lambda^{\pm}_{\text{int}} \in \mathbb{R}$ is considered, i.e., the flow is supposed to remain in the region of strict hyperbolicity.

The stationary solutions of the system satisfy the equations:

$$q_1 = constant, \quad \frac{v_1^2}{2} - \frac{v_2^2}{2} + g' h_1 = constant,$$

$$q_2 = constant, \quad \frac{v_1^2}{2} + g(h_1 + h_2 - H) = constant.$$

In particular, if $q_1 = 0$, $q_2 = 0$, we obtain the solutions:

$$q_1 = 0,\ h_1(x) = constant,\ q_2 = 0,\ h_2(x) - H(x) = constant, \tag{4.22}$$

representing water at rest, that again lie on straight lines of the space of states h_1, q_1, h_2, q_2, H. Therefore, (2.16) is again satisfied by the family of straight segments and, in order to have the well-balanced property for the reconstruction operators, we reconstruct along the variables:

$$q_1, \quad q_2, \quad \eta_1 = h_1 + h_2 - H, \quad \eta_2 = h_2 - H.$$

To calculate the cell averages at the staggered grids, first the equilibrium variables are computed $\bar{q}^n_{1,j+1/2}$, $\bar{q}^n_{2,j+1/2}$, $\bar{\eta}^n_{1,j+1/2}$, $\bar{\eta}^n_{2,j+1/2}$, and then we define:

$$\bar{h}^n_{2,j+1/2} = \bar{\eta}^n_{2,j+1/2} + \bar{H}_{j+1/2}, \quad \bar{h}^n_{1,j+1/2} = \bar{\eta}^n_{1,j+1/2} - \bar{\eta}^n_{2,j+1/2}.$$

Once the new approximations $\bar{u}^{n+1}_{j+1/2}$ have been obtained, the same procedure is used to compute $\bar{u}^{n+2}_{j}$.

Finally, in the RK fluxes of the numerical solution all the conservative terms are written as flux differences but those related to the pressure terms. Using the variables η_1 and η_2 we obtain the following expression:

$$K^{(i)}_{1,j+1/2} = q^{(i)}_{1,j+1} - q^{(i)}_{1,j}, \tag{4.23}$$

$$\begin{aligned} K^{(i)}_{2,j+1/2} = {} & \frac{\left(q^{(i)}_{1,j+1}\right)^2}{h^{(i)}_{1,j+1}} - \frac{\left(q^{(i)}_{1,j}\right)^2}{h^{(i)}_{1,j}} \\ & + \int_{x_j}^{x_{j+1/2}} g\tilde{R}h^{(i)}_1(x)\,\partial_x \tilde{R}\eta^{(i)}_1(x)\,dx + \int_{x_{j+1/2}}^{x_{j+1}} g\tilde{R}h^{(i)}_1(x)\,\partial_x \tilde{R}\eta^{(i)}_1(x)\,dx \\ & + g\frac{h^{(i),-}_{1,j+1/2} + h^{(i),+}_{1,j+1/2}}{2}\left(\eta^{(i),+}_{1,j+1/2} - \eta^{(i),-}_{1,j+1/2}\right) \end{aligned} \tag{4.24}$$

$$K^{(i)}_{3,j+1/2} = q^{(i)}_{2,j+1} - q^{(i)}_{2,j}, \tag{4.25}$$

$$\begin{aligned} K^{(i)}_{4,j+1/2} = & \frac{\left(q^{(i)}_{2,j+1}\right)^2}{h^{(i)}_{2,j+1}} - \frac{\left(q^{(i)}_{2,j}\right)^2}{h^{(i)}_{2,j}} \\ & + \int_{x_j}^{x_{j+1/2}} g\tilde{R}h^{(i)}_2(x)\,\partial_x \tilde{R}\eta^{(i)}_2(x)\,dx + \int_{x_{j+1/2}}^{x_{j+1}} g\tilde{R}h^{(i)}_2(x)\,\partial_x \tilde{R}\eta^{(i)}_2(x)\;dx \\ & + \int_{x_j}^{x_{j+1/2}} rg\tilde{R}h^{(i)}_2(x)\,\partial_x \tilde{R}h^{(i)}_1(x)\,dx + \int_{x_{j+1/2}}^{x_{j+1}} rg\tilde{R}h^{(i)}_2(x)\,\partial_x \tilde{R}h^{(i)}_1(x)\;dx \\ & + gr\frac{h^{(i),-}_{2,j+1/2} + h^{(i),+}_{2,j+1/2}}{2}\left(h^{(i),+}_{1,j+1/2} - h^{(i),-}_{1,j+1/2}\right) \\ & + g\frac{h^{(i),-}_{2,j+1/2} + h^{(i),+}_{2,j+1/2}}{2}\left(\eta^{(i),+}_{2,j+1/2} - \eta^{(i),-}_{2,j+1/2}\right). \end{aligned} \tag{4.26}$$

At steady state, $\tilde{R}\eta_1 \equiv C_1$, $\tilde{R}\eta_2 \equiv C_2$, $\tilde{R}h_1 = C_1 - C_2$ (where C_1 and C_2 denote constants), and all RK fluxes clearly vanish. Thus the time step reduces to $\bar{u}^{n+1}_{j+1/2} = \bar{u}^n_{j+1/2}$, and the way in which the reconstructions at the initial grid are evaluated ensures $\bar{u}^{n+2}_j = \bar{u}^n_j$.

5 Numerical tests

In this Section, the well-balanced properties, accuracy and efficiency of the numerical schemes introduced in the paper are tested for the one layer and the two layer shallow water systems. In order to avoid the appearance of negative values for the water layers thickness when wet/dry fronts are present, the corrections proposed in [6] have been applied.

We have constructed and tested three CRK schemes:

- A first order scheme, based on the explicit Euler method and on piecewise constant reconstructions. No quadrature formula is needed in this case.
- A second order scheme, based on the standard second order TVD-RK scheme and MUSCL reconstructions. Trapezoidal rule ($\mu = 1$) is used as quadrature formula and Version 2 is followed to compute the RK fluxes: the values at the quadrature points are evolved and standard linear interpolation is used.
- A third order scheme, based on the third order TVD-RK scheme [46] and on the third order reconstruction operator PHM (piecewise hyperbolic method) introduced in [28]. Version 2 is followed to compute the RK fluxes. Lagrange quadratic interpolation is used for the reconstruction of the stage values. The quadrature rule is a fourth order formula with 3 nodes ($\mu = 2$) based on numerical extrapolation (see [34] for details).

These schemes are compared with three Roe-type methods (see [9, 37] for details):

- A first order Roe scheme with explicit Euler method in time, denoted by ROE.
- A second order scheme combining the second order TVD-RK scheme and MUSCL reconstructions, denoted by MUSCL-ROE.
- A third order scheme combining the third order TVD-RK scheme and the third order PHM reconstruction operator, denoted by PHM-ROE.

Moreover, a 2D extension of the first and second order CRK schemes on structured meshes have been also implemented. Second order accuracy is achieved using a MUSCL reconstruction operator and the

trapezoidal rule is used as quadrature formula. Here, Version 2 is again followed to compute the RK fluxes.

In all cases, the family of paths considered is the family of straight segments (2.13).

5.1 Test 1: One layer system. Well-balanced property.

The numerical schemes considered in this work solve exactly water at rest solutions. The objective of this first test case is to check numerically this fact. To do it, we consider the interval $[0, 1]$ with depth function $H(x)$ given by an exponential perturbed with random noise (the resulting bottom topography is shown in Fig. 9(a)). As initial conditions we take $h(x, 0) = H(x)$ and $q(x, 0) = 0$, $x \in [0, 1]$. Table 1 shows the L^1 errors obtained with the numerical schemes, for a given mesh with $\Delta x = 0.01$ at $t = 1.0$. The CFL parameter is set to 0.5. As expected, all numerical schemes preserve the steady state up to machine accuracy.

Table 1: Test 1: Water at rest solution. Errors at $t = 1.0$

	1^{st} order		2^{nd} order		3^{rd} order	
	h	q	h	q	h	q
Cells	L_1 error	L_1 error	L_1 error	L_1 error	L_1 error	L_1 error
100	1.12E-15	1.75E-15	2.23E-15	2.17E-15	1.78E-15	2.05E-15

Next, we test the well-balanced property for smooth stationary solutions with $q \neq 0$. We consider the interval $[0, 10]$ with depth function $H(x) = 1 - 0.3e^{-(x-5)^2}$. We consider the subcritical solution corresponding to the integral curve

$$q = 1,\ h - H + \frac{q^2}{2gh^2} = \frac{1}{2g}.$$

.

Table 2 shows the L^1 errors in h obtained for the first, second and third order methods, for five regular meshes with increasing number of cells. The CFL parameter is set to 0.5. The expected orders of accuracy are achieved. Similar results are obtained for the discharge, q. As we see from the data in the table, none of the methods preserves exactly this equilibrium solution, otherwise the errors would be comparable with machine precision; however, the error decreases very quickly when increasing the order of the method.

Table 2: Test 1: Errors and order.

	1^{st} order		2^{nd} order		3^{rd} order	
Cells	L_1 error	L_1 order	L_1 error	L_1 order	L_1 error	L_1 order
20	9.39E-02	-	5.62E-02	-	9.09E-02	-
40	5.89E-02	0.67	2.66E-02	1.08	2.58E-02	1.81
80	3.97E-02	0.57	8.38E-03	1.66	3.84E-03	2.75
160	2.33E-02	0.77	1.98E-03	2.08	5.68E-04	2.76
320	1.24E-02	0.91	4.41E-04	2.17	8.47E-05	2.75

5.2 Test 2: One layer system. Well balanced property for a non-smooth solution.

This test is designed to assess the long time behavior of the solution and the convergence to a steady state including a regular transition and a shock. The computational domain is the interval $[0, 20]$. The

bottom topography is given by the function

$$H(x) = \begin{cases} 0.05(x-10)^2, & \text{if } 8 < x < 12; \\ \\ 0.2, & \text{otherwise.} \end{cases}$$

The initial conditions are $h(x,0) = 0.13 + H(x)$, $q(x,0) = 0.18$, and the boundary conditions are $q(0,t) = 0.18$, $h(0,t) = 0.33$. The CFL parameter is set to 0.5.

A reference solution is computed with ROE scheme with a mesh of 6400 points. Table 3 shows the L^1 errors on h obtained for five regular meshes with increasing number of cells. Again, similar results are obtained for q. Figures 3(a) and 3(b) show the comparison of the numerical results with the reference solution at time $t = 200$ with the coarsest grid $\Delta x = 1/10$. In this case, as the steady state solution is not regular, some accuracy loss can be observed. Nevertheless notice that, for a fixed mesh width, the error decreases as the the order of accuracy increases, so that even though full accuracy is not achieved, still higher order schemes provide a better resolution.

Table 3: Test 2: Errors and order at t=200.

	1^{st} order		2^{nd} order		3^{rd} order	
Cells	L_1 error	L_1 order	L_1 error	L_1 order	L_1 error	L_1 order
50	4.98E-01	-	1.61E-01	-	4.90E-01	-
100	3.05E-01	0.71	4.94E-02	1.70	3.32E-02	3.88
200	1.79E-01	0.77	1.81E-02	1.45	9.16E-03	1.86
400	9.70E-02	0.88	7.04E-03	1.36	3.33E-03	1.46

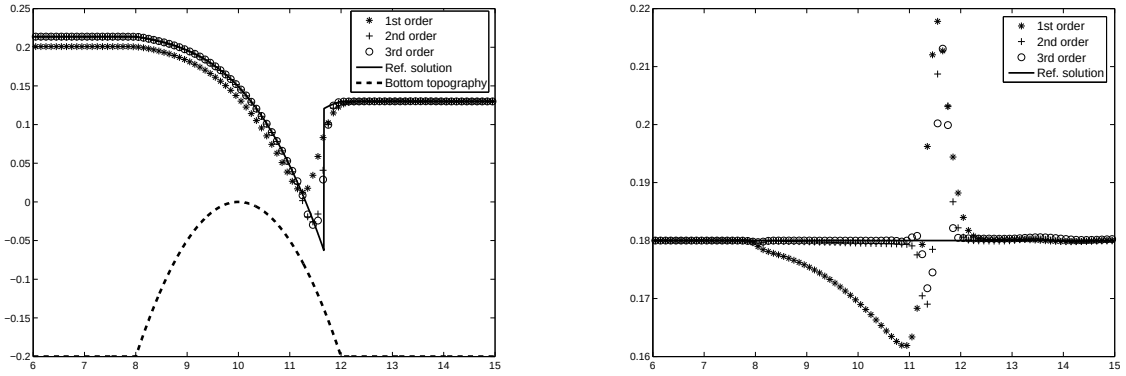

(a) Free surface (b) Discharge

Figure 3: Test 2: Comparison with the reference solution at $t = 200$ with $\Delta x = 1/10$.

5.3 Test 3. Order of accuracy: one layer system

This test is designed to evaluate the accuracy of the schemes for smooth time-dependent solutions. We consider the interval $[0, 20]$ with depth function $H(x) = 5.0 - e^{-(x-10)^2}$. The initial condition is $q(x,0) = 0$ and

$$h(x,0) = H(x) + 0.1 \sin\left(\frac{\pi x}{5}\right).$$

The final time is $t = 0.1$. Periodic boundary conditions are considered. The CFL parameter is set to 0.3.

A reference solution is computed with PHM-ROE scheme using a mesh of 6400 points. Table 4 shows the L^1 errors and the orders obtained on the variable h. Similar results are observed on q. As expected, first, second and third order accuracy are achieved.

Table 4: Test 3: Errors and order at t=0.1.

	1^{st} order		2^{nd} order		3^{rd} order	
Cells	L_1 error	L_1 order	L_1 error	L_1 order	L_1 error	L_1 order
50	2.85E-01	-	6.17E-02	-	2.85E-01	-
100	1.53E-01	0.90	1.66E-02	1.90	5.41E-02	2.40
200	7.95E-02	0.95	4.39E-03	1.92	1.97E-03	4.78
400	3.99E-02	0.99	1.16E-03	1.92	2.52E-04	2.97
800	2.02E-02	0.99	2.99E-04	1.96	3.23E-05	2.97

Figure 4 shows the CPU versus the error (logarithmic scale) for the first, second and third order CRK schemes and first, second and third order Roe schemes. Note that the first order Roe scheme is more efficient than the first order CRK, but, when the second or third order version of the schemes are used, both CRK and Roe approximately provide the same efficiency for a fixed error. It is clear from this Figure that the second and third order CRK scheme are a competitive choice in comparison with the corresponding Roe scheme, when unsteady solutions are considered. Note that the results are similar to those obtained with the schemes introduced in [12].

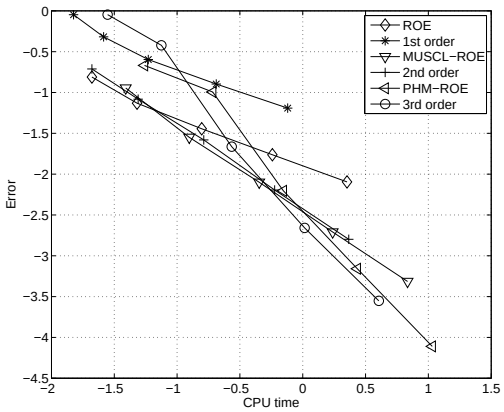

Figure 4: Test 3: CPU vs. Error (log scale).

5.4 Test 4: Propagation of perturbations.

In order to test the performance of the schemes on a rapidly varying flow over a smooth bed, we consider a test proposed by LeVeque in [24]. Specifically, a steady state solution is perturbed by a pulse that splits into two waves propagating in opposite directions over a continuous bed. The left-going wave travels over a horizontal bottom while the right-going wave propagates over a bump. The computational domain is the interval $[0, 2]$. Outflow boundary conditions have been considered. The bottom topography is given by the function

$$H(x) = \begin{cases} 1 - 0.25(\cos(10\pi(x - 0.5)) + 1), & \text{if } 1.4 < x < 1.6; \\ \\ 1, & \text{otherwise.} \end{cases}$$

The initial data is $q(x,0) = 0$, and

$$h(x,0) = \begin{cases} H(x) + \Delta h, & \text{if } 1.1 < x < 1.2; \\ \\ H(x), & \text{otherwise.} \end{cases}$$

Here Δh is the height of the perturbation, that takes the value $\Delta h = 0.001$ (small pulse). Free boundary conditions are imposed and the CFL parameter is set to 0.5.

A reference solution is computed with ROE scheme using a mesh of 6400 cells. In Figure 5 we compare the results obtained for first, second and third order schemes with the reference solution at time $t = 0.2$ taking $\Delta x = 1/80$.

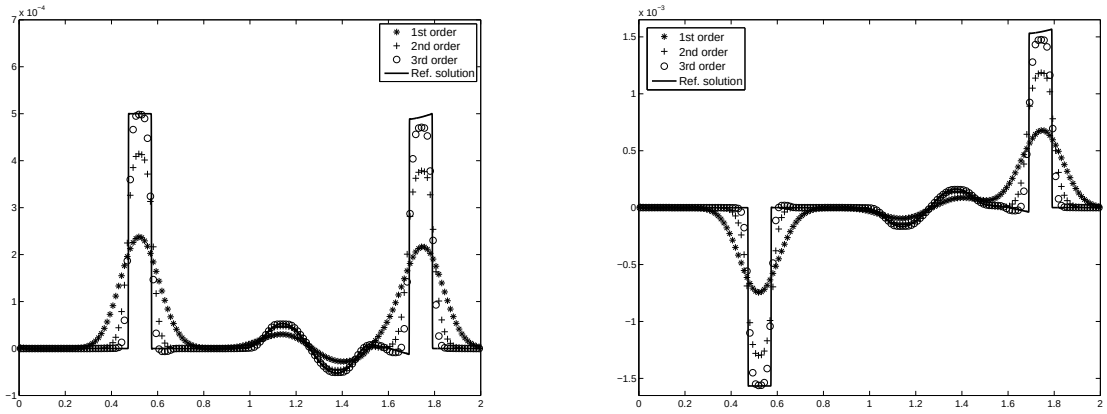

(a) Free surface. (b) Discharge.

Figure 5: Test 4: Comparison with the reference solution at t=0.2 with $\Delta x = 1/80$.

5.5 Test 5: Wet/dry fronts in a non-flat basin.

In order to test the performance of the schemes in the presence of wet/dry zones, we consider a problem proposed by Gallouët et al. in [19], specifically designed to assess the behaviour on drying a non-flat basin. In this test case, a dry bed is formed in the middle of two rarefaction waves travelling in opposite directions. The generation of the dry bed makes this problem numerically difficult, especially when the left-going rarefaction wave propagates over the step. The computational domain is the interval $[0, 25]$. The bottom topography is given by the function

$$H(x) = \begin{cases} 13, & \text{if } 25/3 < x < 25/2; \\ \\ 14, & \text{otherwise.} \end{cases}$$

The initial condition is

$$h(x,0) = H(x) - 4, \qquad q(x,0) = \begin{cases} -300, & \text{if } \frac{50}{3} \leq x; \\ \\ 300, & \text{if } \frac{50}{3} > x. \end{cases}.$$

A reference solution is computed using ROE scheme with a mesh of 6400 points. Figure 6 is a zoom of the left going wave and it shows the comparison of the numerical results obtained with the reference solution at time $t = 0.25$ taking $\Delta x = 1/16$, yielding 400 points. As it can be seen, the numerical schemes

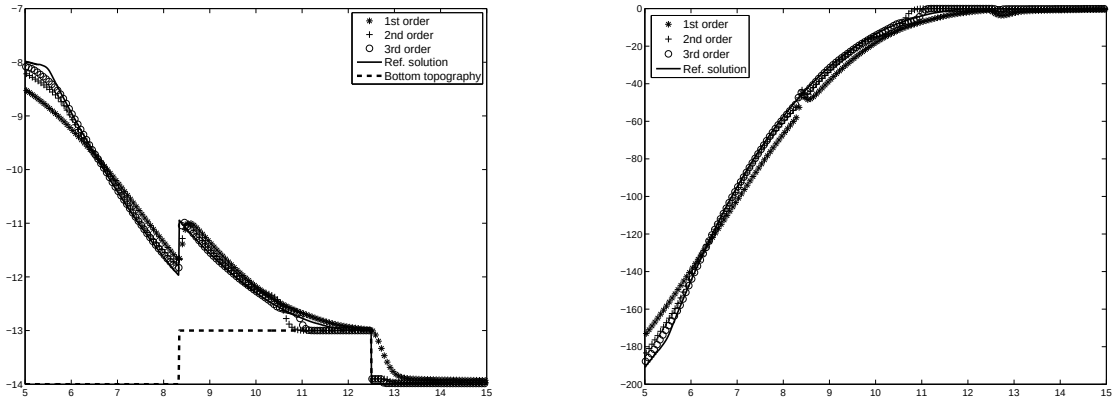

(a) Free surface.

(b) Discharge.

Figure 6: Test 5: Comparison with the reference solution at t=0.25 with $\Delta x = 1/16$.

can run this difficult test, but some small differences can be observed close to the step. Moreover, the first order numerical scheme does not completely dry the area placed to the right of the step, while the second and third order tend to overdry the region just to the left of the right edge of the step. This is due to an overestimation of the velocities: the computation of accurate approximation of the velocity with a high-order reconstruction operator near a wet/dry front is a difficult task which is out of the scope of this paper.

5.6 Test 6: 2D Circular dam-break problem

We consider the following 2D dam break problem proposed in [7]: the domain is the square $D = [0, 2] \times [0, 2]$. The bottom topography function is given by:

$$H(x, y) = 0.6 - \frac{1}{8} \left(\cos(2\pi(x - 0.5)) + 1\right) \left(\cos(2\pi y) + 1\right),$$

and the initial condition is:

$$h(x, y, 0) = \begin{cases} 0.5 + H(x, y) & \text{if } (x - 1.25)^2 + (y - 1)^2 \leq (0.1)^2, \\ H(x, y) & \text{otherwise,} \end{cases}, \qquad \vec{q} = 0.$$

and $\vec{q} = 0$. Wall boundary conditions are set at $y = 0$ and $y = 2$ and free boundary conditions at $x = 0$ and $x = 2$. The CFL is set to 0.25 and $\Delta x = \Delta y = 0.02$. A reference solution is computed with first order Roe scheme with $\Delta x = \Delta y = 0.0025$.

Figure 7 shows the free surface computed with the first and second order CRK scheme at different times ($t = 0.1$ and 0.2 s). Note that the second order scheme reduces sharply the numerical diffusion introduced by the first order CRK scheme, as expected. Thsi behavior is even more apparent in Figure 8 which contains a comparison between the two numerical solutions and a reference solution at the longitudinal section $y = 1$.

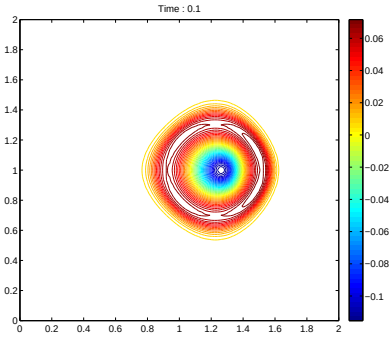

(a) $t = 0.1$

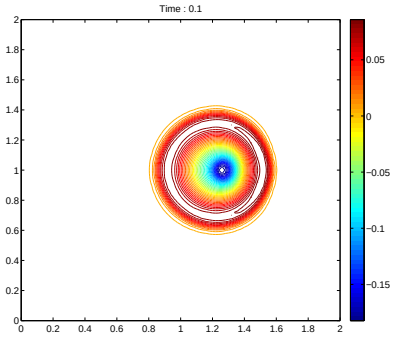

(b) $t = 0.1$

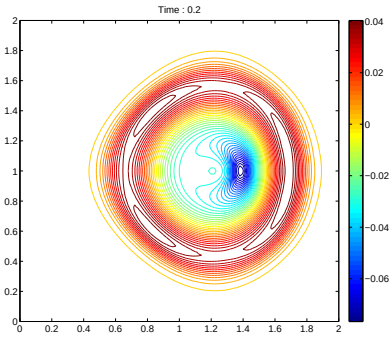

(c) $t = 0.2$

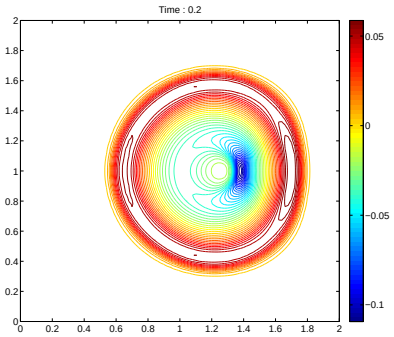

(d) $t = 0.2$

Figure 7: Test 6: Circular dam-break. Evolution of the free surface at different time steps. Comparison between first (left) and second (right) order CRK schemes.

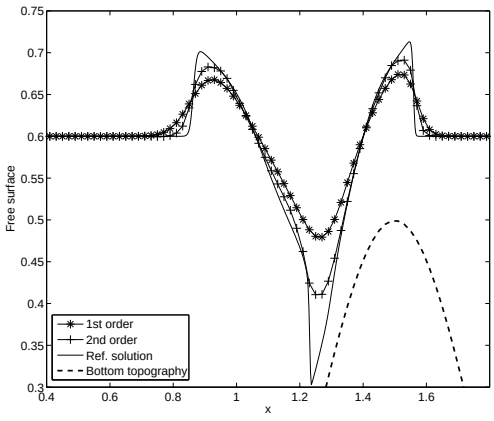

(a) $t = 0.1$

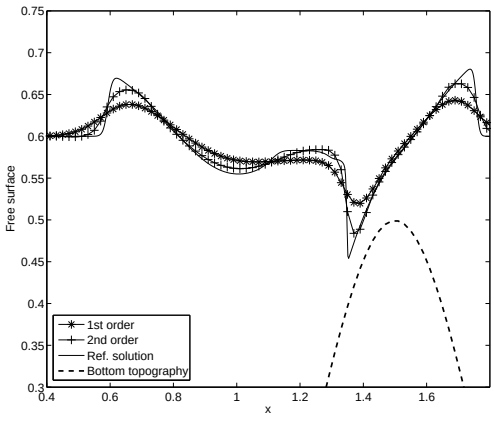

(b) $t = 0.2$

Figure 8: Test 6: Circular dam-break. Longitudinal cut at $y = 1$ of the evolution of the free surface at different time steps. Comparison between first and second order CRK schemes and a reference solution computed with Roe scheme.

5.7 Test 7: two-layer system. Well-balanced property.

As for the one-layer problem, the purpose of this test is to check numerically that all schemes solve exactly water at rest solutions for the two-layer system. We consider the same set up defined in Test 1. As initial conditions we take $h_1(x,0) = 1.0$, $h_2(x,0) = H(x)$, and $q_1(x,0) = q_2(x,0) = 0$, $x \in [0,1]$. The CFL parameter is set to 0.5. Table 5 shows the L^1 errors obtained with the numerical schemes, for a given mesh with $\Delta x = 0.01$. As expected, all numerical schemes preserve the steady state up to machine accuracy, even with such a rough bottom: see Table 5 . Figure 9 shows the free surface, the interface, and the discharges at time $t = 1.0$.

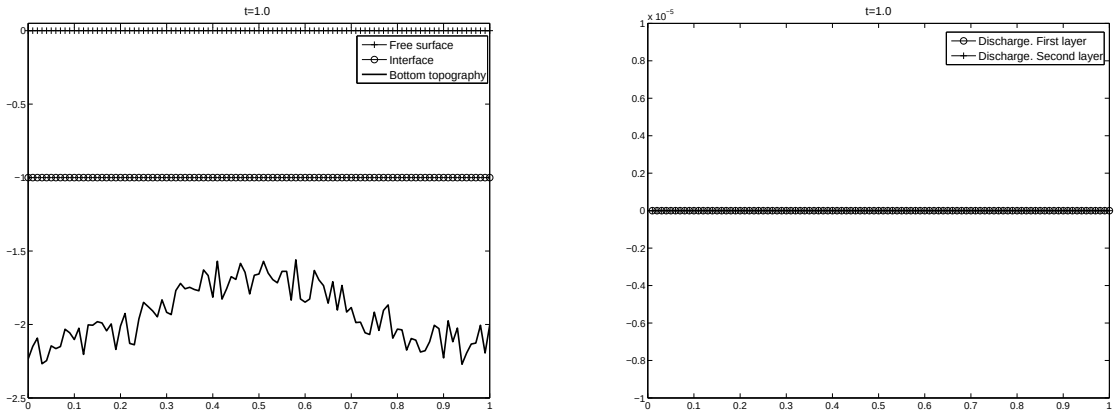

(a) Free surface - Interface -Bottom topography

(b) Discharge. First and second layers

Figure 9: Test 7: water at rest solution at $t = 1.0$ with $\Delta x = 0.01$.

Table 5: Test 7: Water at rest solution. Errors.

	1^{st} order	2^{nd} order	3^{rd} order
Cells	error	error	error
100	1.07E-15	1.63E-15	1.23E-15

5.8 Test 8: Order of accuracy: two layer system

This test is designed to evaluate the accuracy of the schemes for smooth time-dependent solutions of the non-homogeneous two-layer shallow water system. We consider the interval $[0, 20]$ with depth function:

$$H(x) = 5.0 - e^{-(x-10)^2}.$$

The initial condition is $q_1(x,0) = q_2(x,0) = 0$, $h_1(x,0) = 1.0$ and

$$h_2(x,0) = H(x) + 0.1 \sin\left(\frac{\pi x}{5}\right).$$

The final time is $t = 0.1$. Periodic boundary conditions are considered. The CFL parameter is set to 0.2.

A reference solution is computed with ROE scheme using a mesh of 6400 points. Table 6 shows the L^1 errors for CRK and Roe schemes of the same order (only the maximum error in the four unknowns is shown), together with the speedup obtained using the CRK scheme with respect to the Roe scheme of the same order, for five regular meshes with increasing number of cells. All schemes achieve the expected

Table 6: Test 8: Errors for CRK and ROE schemes together with the Speedup (Sp) with respect to Roe scheme at t=0.1.

	1^{st} order			2^{nd} order			3^{rd} order		
Cells	CRK	ROE	Sp	CRK	ROE	Sp	CRK	ROE	Sp
50	1.02	4.87E-01	1.96	2.01E-01	1.09E-01	2.43	1.32E-01	2.37E-01	2.22
100	5.45E-01	2.96E-01	2.76	8.60E-02	2.63E-02	2.90	4.71E-02	1.70E-01	2.34
200	2.82E-01	1.52E-01	3.44	2.66E-02	7.10E-03	3.12	1.32E-02	6.85E-03	2.43
400	1.43E-01	7.59E-02	3.72	6.52E-03	1.78E-03	3.20	2.87E-03	8.95E-04	2.46
800	7.01E-02	3.61E-02	3.75	1.63E-03	4.45E-04	3.20	4.08E-04	1.20E-04	2.48

order of accuracy. Note that the errors for Roe schemes are smaller than the ones obtained by comparable central schemes on the same grid.

However, we note that the speedup is about 3.75 for the first order numerical scheme, 3.20 for the second order one, and 2.5 for the third order one. This CPU time reduction is due to the fact that the implementation of Roe schemes requires the explicit knowledge of the eigenstructure of the intermediate matrices, which is performed numerically as there is not an easy analytical expression available for the eigenvalues and eigenvectors of the system. Therefore, if we compute the error as a function of the CPU time, the CRK schemes proposed in this work become competitive. Figure 10 shows the CPU versus the error for the six schemes. Note that the efficiency is similar for CRK and Roe-type schemes with the same order of accuracy, even in the first order case.

Figure 10 contains much interesting information. First of all it clearly shows the advantage in terms of CPU time of using a second order scheme rather than a first order scheme. The situation is more complex for the third order scheme: the higher order scheme in this test produces comparable accuracy with the same effort of a second order scheme. On the other hand, we expect a better resolution of discontinuities with the higher order method, so the third order scheme seems still to be preferable. Secondly, we note that the central scheme provides comparable errors for a fixed CPU time to a Roe type scheme of the same order. Thus the artificial diffusion induced by the central approach is compensated by the fact that the scheme is faster than Roe for a given mesh size. In other words, the central scheme is convenient over a Roe type method when the eigenstructure of the system is complicated, slowing down the computation of Roe numerical fluxes. Note that the results are similar to those obtained with the schemes introduced in [12].

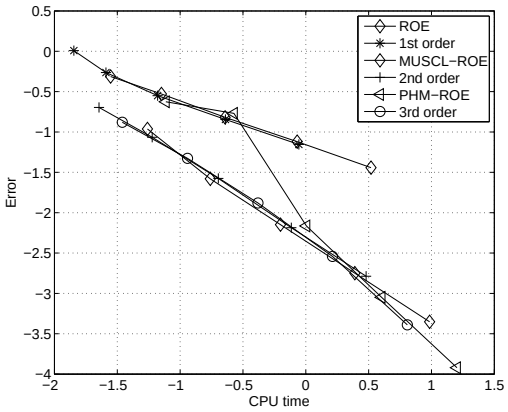

Figure 10: Test 8: CPU vs. Error (log scale).

5.9 Test 9: Two-layer shallow water. Well-balanced property for a non-smooth solution

In this test the computational domain is the interval $[0, 10]$. The bottom topography is given by the function

$$H(x) = 1.0 - e^{-(x-5.0)^2}.$$

The initial condition is $q_1(x, 0) = q_2(x, 0) = 0$, and

$$h_1(x,0) = \begin{cases} 1.0 & \text{if } x < 5, \\ 0.0 & \text{otherwise,} \end{cases} \qquad h_2(x,0) = \begin{cases} 1.0 - e^{-(x-5)^2} & \text{if } x < 5, \\ 2.0 - e^{-(x-5)^2} & \text{otherwise.} \end{cases}$$

As boundary conditions, the relation $q_1(\cdot, t) = -q_2(\cdot, t)$ is imposed at $x = 0$, and the free surface is fixed to $z = 1$ at $x = 10$, that is $h_1(10, t) + h_2(10, t) - H(x) = 1.0$. The CFL parameter is set to 0.5 and $r = 0.98$.

A reference solution is computed with PHM-ROE scheme using a mesh of 3200 points. Figure 11 shows the comparison of the numerical solutions obtained with the reference solution at time $t = 300$ taking $\Delta x = 1/40$, resulting in 400 points.

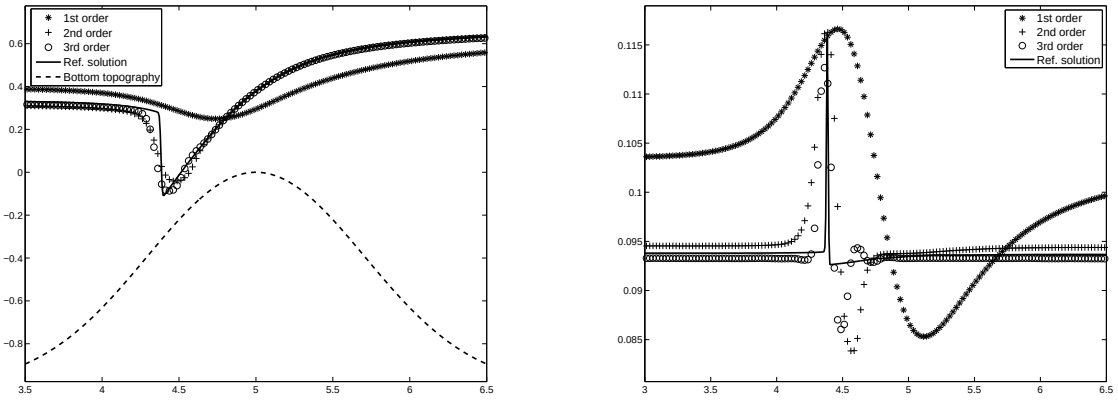

(a) Interface (zoom)

(b) Discharge (zoom). First layer

Figure 11: Test 9: Comparison with the reference solution at time $t = 300$ with $\Delta x = 1/40$.

5.10 Test 10: Internal dam-break problem.

This test is designed to evaluate the accuracy of the schemes for non-regular time-dependent solutions over a flat bottom. We consider the interval $[0, 10]$ along a rectangular channel.

The initial conditions are $q_1(x, 0) = q_2(x, 0) = 0$,

$$h_1(x,0) = \begin{cases} 0.2, & \text{if } x < 5, \\ \\ 0.8, & \text{otherwise,} \end{cases} \qquad h_2(x,0) = \begin{cases} 0.8, & \text{if } x < 5, \\ \\ 0.2, & \text{otherwise.} \end{cases}$$

Free boundary conditions are considered. The CFL parameter is set to 0.5 and $r = 0.98$. A reference solution is computed with PHM-ROE scheme using a mesh of 3200 points.

Figure 12 shows the comparison of the numerical results with the reference solution at time $t = 10$ taking $\Delta x = 1/20$.

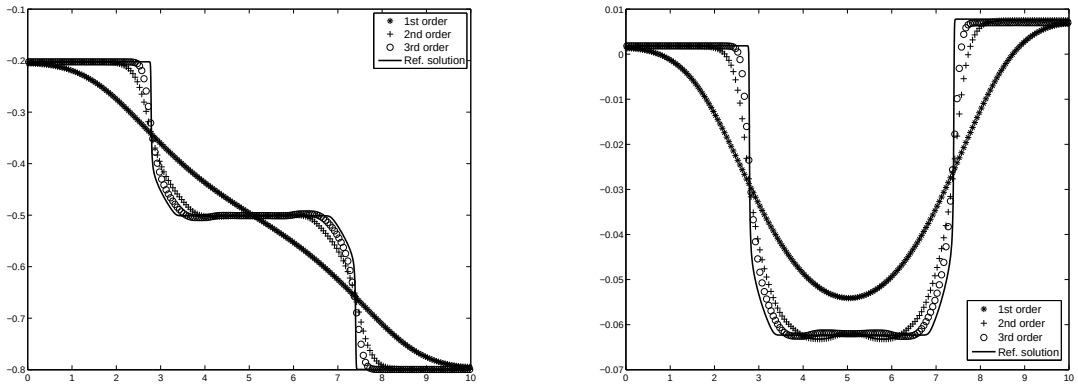

(a) Interface.

(b) Discharge. First layer.

Figure 12: Test 10: Comparison with the reference solution at $t = 10$ s with $\Delta x = 1/20$.

Although we know from the theoretical analysis (see [8]) that each scheme might converge to different shock speeds (as each one of them has a different numerical viscosity and thus provides a different regularization to the nonconservative system), the actual differences we observe in computations are indeed very small.

5.11 Test 11: 2D Internal circular dam-break problem

Finally, let us consider the domain $[-2, 2] \times [-2, 2]$ with the following bottom topography:

$$H(x, y) = 2.0 - 0.5e^{-5(x^2+y^2)}.$$

As initial condition we set $\vec{q}_1 = \vec{q}_2 = 0$ and

$$h_2(x, y, 0) = \begin{cases} 0.2 - 0.5e^{-5(x^2+y^2)} & \text{if } (x^2 + y^2) > 1, \\ 1.8 - 0.5e^{-5(x^2+y^2)} & \text{otherwise,} \end{cases}$$

$$h_1(x, y, 0) = \begin{cases} 1.8 & \text{if } (x^2 + y^2) > 1, \\ 0.2 & \text{otherwise.} \end{cases}$$

The CFL is set to 0.25 and $\Delta x = \Delta y = 0.02$. A reference solution is computed with first order Roe scheme with $\Delta x = \Delta y = 0.005$.

Figure 13 shows the evolution of the interface ($\eta_2 = h_2 - H$) for the first (left column) and second (right column) order CRK schemes. Figure 14 shows a comparison between the computed interface obtained with first and second order CRK schemes with the reference solution computed with first order Roe scheme with a fine mesh at the longitudinal section $y = 0$. Finally, Figure 15 shows the evolution of the free surface ($\eta_1 = h_1 + h_2 - H$) for the first (left column) and second (right column) order CRK schemes. Observe that the second order scheme is able to capture the complicated structure of the free surface waves after several reflections at the closed boundaries. Again, the second order scheme is more accurate than the first order, as expected. Concerning the speedup of CRK with respect to Roe scheme, it is approximately a factor of 3.7 for the first order scheme and 3.2 for the second order case.

6 Conclusions

In this paper we show how to construct high order well balanced central schemes on staggered grids for hyperbolic systems, possibly with non-conservative terms. The proposed schemes preserve static equilib-

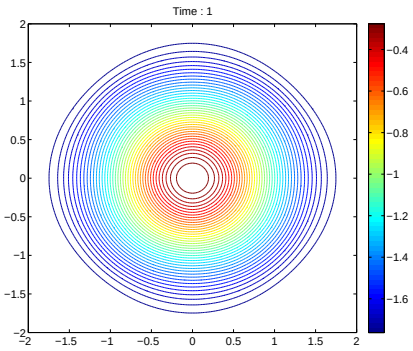

(a) Interface (first order) at $t = 1$

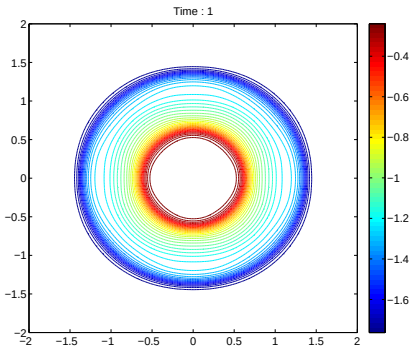

(b) Interface (second order) at $t = 1$

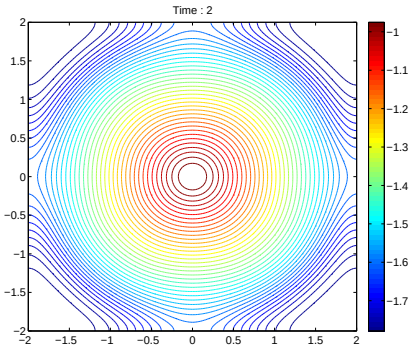

(c) Interface (first order) at $t = 2$

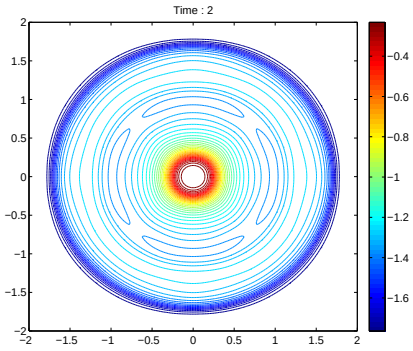

(d) Interface (second order) at $t = 2$

Figure 13: Test 11: Evolution of the interface: Left (first order), right (second order) with $\Delta x = 0.02$.

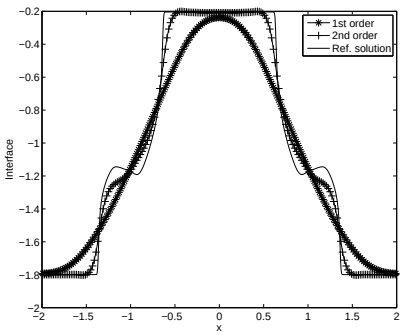

(a) $t = 1$

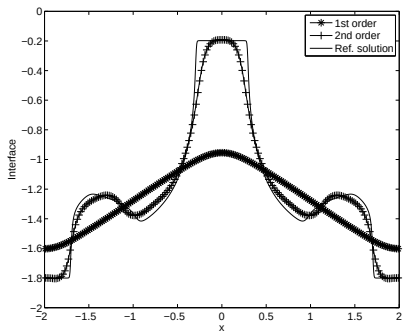

(b) $t = 2$

Figure 14: Test 11: Internal circular dam-break. Longitudinal cut at $y = 0$ of the evolution of the interface at different time steps. Comparison between first and second order CRK schemes and a reference solution computed with Roe scheme.

ria. The central approach allows very efficient implementation, because it requires minimal characteristic information from the system. Several numerical tests show the effectiveness of the proposed scheme, which compete favorably with state-of-the-art schemes of the same order. In fact, we obtain similar efficiencies to those obtained with path-conservative schemes introduced in [12].

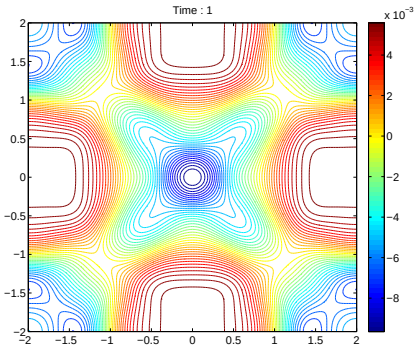

(a) Free surface (first order) at $t = 1$

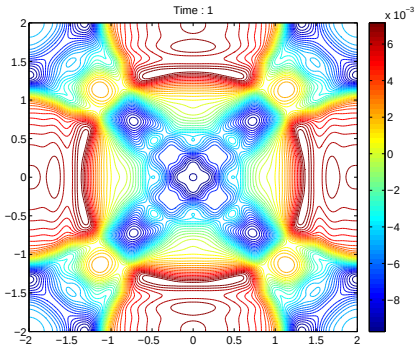

(b) Free surface (second order) at $t = 1$

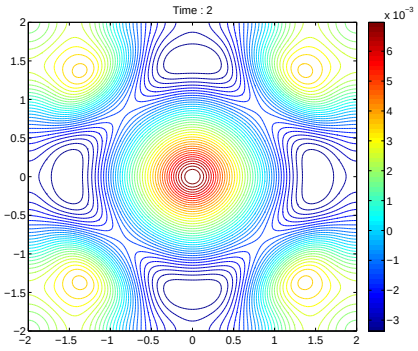

(c) Free surface (first order) at $t = 2$

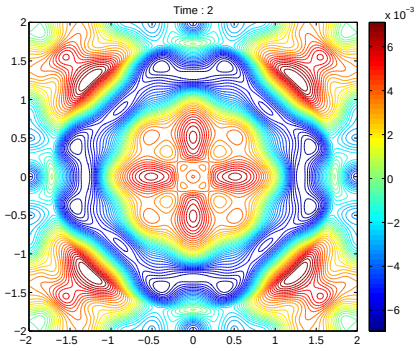

(d) Free surface (second order) at $t = 2$

Figure 15: Test 11: Evolution of the free surface: Left (first order), right (second order) with $\Delta x = 0.02$.

Our tests show that second and third order central methods based on staggered grids provides comparable errors for a fixed CPU time with respect to path conservative schemes based on the Roe numerical flux, for the one and two layers shallow water models. Thus in this case the artificial viscosity introduced by central schemes on staggered grids with respect to standard solvers is compensated by the fact that central schemes are much faster than Roe type schemes on a given grid. We believe that the break-even point between central and upwind schemes depends on the complexity of the system of equations. Central schemes seem to have an edge over upwind schemes when the eigenstructure of the system of equations requires a strong computational effort. A further advantage of the central approach is due to its ease of design. Since it is faster to implement a central scheme than a Roe type scheme, central schemes are suited when the eigenstructure of the flux matrix is complex, or when one wishes to test several different models, which can be implemented with rather minor modifications of the code.

Acknowledgments

This research has been partially supported by the Spanish Government Research project MTM2009-11293 and the Italy-Spain Integrated Action HI2008-0122. The numerical computations have been performed at the Laboratory of Numerical Methods of the University of Málaga.

References

[1] Abgrall R., Karni S., *A comment on the computation of non-conservative products.* J. Comput. Phys., 45 (2010), 382–403.

[2] Bianco F., Puppo G., Russo G., *High Order Central Schemes for Hyperbolic Systems of Conservation Laws*, SIAM J. Sci. Comp., 21 (1999) no 1, 294–322.

[3] Bouchut, F. *Nonlinear stability of finite volume methods for hyperbolic conservation laws, and well-balanced schemes for sources.* Birkhäuser (2004).

[4] Bouchut, F., Morales De Luna T., *An entropy satisfyig scheme for two layers shallow water equations with uncoupled treatment*, Math. Mod. Num. Anal. *Add the year!!*

[5] Castro M.J., Fernández-Nieto, E.D., Ferreiro A., *Sediment transport models in Shallow Water equations and numerical approach by high order finite volume methods*, Comput Fluids, 37 (2008), 299–316.

[6] Castro M.J., Ferreiro A., García-Rodriguez J.A., González J.M., Macías J., Parés C., Vázquez-Cendón M.E., *On the numerical treatment of wet/dry fronts in shallow flows: application to one-layer and two-layer 1-D shallow water system.* Math. and Comp. model., 42 (2005), 419–439.

[7] M.J. Castro, E.D. Fernández, A.M.Ferreiro, J.A. García, and C. Parés *High order extensions of Roe schemes for two dimensional nonconservative hyperbolic systems.* Jour. Sci. Comp. 39: 67–114, 2009.

[8] Castro M.J., LeFloch P.G., Muñoz M.L., Parés C., *Why many theories of shock waves are necessary: convergence error in formally path-consistent schemes.* J. Comput. Phys 227 (2008), 8107–8129.

[9] Castro M.J., Gallardo J.M., Parés C., *High order finite volume schemes based on reconstruction of states for solving hyperbolic systems with nonconservative products. Applications to shallow water systems.* Math. Comp., 75 (2006), 1103-1134.

[10] Castro M.J., Gallardo J.M., López J.A., Parés C., *Well-balanced high order extensions of Godunov's method for semilinear balance laws.* SIAM J. Num. Anal.,46(2008): 1012–1039.

[11] Castro M.J., Macías J., Parés C., *A Q-Scheme for a class of systems of coupled conservation laws with source term. Application to a two-layer 1-D shallow water system.* Math. Mod. Num. Anal., 35 (2001), 107–127.

[12] Castro M.J., Pardo A., Parés C., Toro E.F. *On some fast well-balanced first order solvers for nonconservative systems.* Math. of Comp. 79 (2010), 1427-1472.

[13] Dal Maso G., LeFloch P.G., Murat F. *Definition and weak stability of nonconservative products.* J. Math. Pures Appl. 74 (1995), 483–548.

[14] Dumbser, M., Castro, M.J., Parés, C., Toro, E. F., *ADER schemes on unstructured meshes for nonconservative hyperbolic systems: Applications to geophysical flows.* Comp. & Fluids, 38 (2009), 1731–1748.

[15] Dumbser M., Hidalgo A., Castro M.J., Parés C., Toro E.F., *FORCE schemes on unstructured meshes II: Non-conservative hyperbolic systems.* Comp. Meth. Appl. Mech. Eng. 199 (2010), 625–647.

[16] Colella P., Woodward P.R., *Piecewise parabolic method (PPM) for gas-dynamical simulations.* J. Comput. Phys. 54 (1984), 174–201.

[17] Dumbser, M. Toro, E. *A simple extension of the Osher Riemann solver to non-conservative Hyperbolic systems*, J. Sci. Comp. 48, (2011), 70–88.

[18] Gallardo J.M., Parés C., Castro M.J., *On a well-balanced high-order finite volume scheme for shallow water equations with topography and dry areas.* J. Comput. Phys. 227(2007): 574–601.

[19] Gallouët T., Hèrard J.M., Seguin N., *Some approximate Godunov schemes to compute shallow-water equations with topography.* Computers and Fluids 32 (2003): 479–513.

[20] Harten A., Engquist B., Osher S., Chakravarthy S., *Uniformly High Order Accurate Essentially Non Oscillatory Schemes III*, J. Comput. Phys. 71 (1987), 231–303.

[21] Hou T.Y., LeFloch P.G., *Why nonconservative schemes converge to wrong solutions: error analysis.* Math. Comp. 62 (1994), 497–530.

[22] Jiang G.-S., Shu C.-W., *Efficient Implementation of Weighted ENO Schemes*, J. Comput. Phys., 126 (1996), 202–228.

[23] Jiang G.S., Tadmor E., *Nonoscillatory central schemes for multidimensional hyperbolic conservation laws*, SIAM J. Sci. Comp. 19 (1998), 1892–1917.

[24] LeVeque R.J., *Balancing source terms and flux gradients in high-resolution Godunov methods: the quasi-steady wave-propagation algorithm.* J. Comp. Phys. 146 (1998): 346–365.

[25] LeVeque R.J., *Finite Volume Methods for Hyperbolic Problems*, Cambridge Texts in Applied Mathematics, Cambridge University Press, Cambridge, UK (2002).

[26] Levy D., Puppo G., Russo G., *Central WENO Schemes for Hyperbolic Systems of Conservation Laws*, Math. Model. and Numer. Anal., 33 (1999) no. 3, 547–571.

[27] Lie K.A., Noelle S., *An improved quadrature rule for the flux-computation in staggered central difference schemes in multidimensions*, J. Sci. Comp., 18, (2002), 69–81.

[28] Marquina A., *Local piecewise hyperbolic reconstructions for nonlinear scalar conservation laws*, SIAM J. Sci. Comp 15 (1994) 892–915.

[29] Muñoz-Ruiz M.L., Parés C., *Godunov method for nonconservative hyperbolic systems*, Math. Model. Numer. Anal. 41 (2007), 169–185.

[30] Muñoz-Ruiz M.L., Parés C., *On some difficulties of the numerical approximation of nonconservative hyperbolic systems*, Bol. Soc. Esp. Mat. Apl, 47 (2009), 23–52.

[31] Morales de Luna T., Castro M. J., Parés C., Fernández-Nieto, E. D., *On a shallow water model for the simulation of turbidity currents.* Comm. Comp. Phys. 6 (2009), 848–882.

[32] Muñoz-Ruiz M.L., Parés C., *On the convergence and well-balanced property of path-conservative numerical schemes for systems of balance laws.* J. Sci. Comput. DOI: 10.1007/s10915-010-9425-7.

[33] Nessyahu H., Tadmor E., *Non-oscillatory Central Differencing for Hyperbolic Conservation Laws*, J. Comput. Phys. 87 (1960) no. 2, 408–463.

[34] Noelle S., Pankratz N., Puppo G., Natvig J.R. *Well-balanced finite volume schemes of arbitrary order of accuracy for shallow water flows.* J. Comput. Phys. 213 (2006), 474–499.

[35] Noelle S., Xing Y., Shu C.W. *High order well balanced schemes*, in: Puppo G., Russo G. eds. *Numerical Methods for Balance Laws*, Quaderni di Matematica, Aracne (2010).

[36] Noelle S., Xing Y., Shu C.-W. *High order well-balanced finite volume WENO schemes for shallow water equation with moving water.* J. Comput. Phys. 226 (2007),29–59.

[37] Parés C., Castro M.J., *On the well-balanced property of Roe's method for nonconservative hyperbolic systems. Applications to Shallow-Water Systems.* M2AN, 38 (2004) no. 5, 821–852.

[38] Parés C., *Numerical methods for nonconservative hyperbolic systems: a theoretical framework.* SIAM J. Num. Anal. 44 (2006) no. 1, 300–321.

[39] Parés, C., *Path conservative numerical methods for nonconservative hyperbolic systems*, in: Puppo G., Russo G. eds. *Numerical Methods for Balance Laws*, Quaderni di Matematica, Aracne (2010).

[40] Pareschi L., Puppo G., Russo C. *Central Runge-Kutta Schemes for Conservation Laws.*, SIAM J. Sci. Comput. 26 (2005), no. 3, 979–999.

[41] Qiu J., and Shu C.W., *On the construction, comparison, and local characteristic decomposition for high order central WENO schemes*, J. Comput. Phys. 183 (2002), 187–209.

[42] Russo G., Khe A., *High order well balanced schemes for systems of balance laws*, in: *Hyperbolic problems: theory, numerics and applications*, 919–928,. Proc. Sympos.Appl. Math., 67, Part 2, Amer. Math. Soc., Providence, RI, (2009).

[43] Russo G., Khe A., *High Order Well-Balanced Schemes Based on Numerical Reconstruction of the Equilibrium Variables*, in: *Proceedings WASCOM 2009, Waves and Stability in Continuous Media*, Palermo (2009).

[44] Schijf J.B., and Schonfeld J.C., *Theoretical considerations on the motion of salt and fresh water.* In Proc. of the Minn. Int. Hydraulics Conv., 321–333. Joint meeting IAHR and Hyd. Div. ASCE., Sept. 1953.

[45] Shu C.-W., *Essentially Non-Oscillatory and Weighted Essentially Non-Oscillatory Schemes for Hyperbolic Conservation Laws* in Advanced Numerical Approximation of Nonlinear Hyperbolic Equations, Lecture Notes in Mathematics (editor: A. Quarteroni), Springer, Berlin, 1998.

[46] Shu C.-W., Osher S., *Efficient Implementation of Essentially Non-oscillatory Shock-Capturing Schemes, II*, J. Comput. Phys. 83 (1989), 32–78.

[47] Tadmor E., *Approximate Solutions of Nonlinear Conservation Laws*, in Advanced Numerical Approximation of Nonlinear Hyperbolic Equations, Lecture Notes in Mathematics (editor: A. Quarteroni), Springer, Berlin, 1998.

[48] Toumi I., *A weak formulation of Roe's approximate Riemann solver*, J. Comput. Phys. 102 (1992), 360–373.

[49] Van Leer B., *Towards the ultimate conservative difference scheme. V. A second-order sequel to Godunov's method.* J. Comput. Phys. 32 (1979), 101– 136.